

# GEOLOGIC MAP OF THE COLOCKUM PASS SE 7.5-MINUTE QUADRANGLE, KITITITAS COUNTY, WASHINGTON

by Andrew J. Sadowski and Todd R. Lau

WASHINGTON  
GEOLOGICAL SURVEY  
Map Series 2022-05  
December 2022

INTERNALLY REVIEWED



WASHINGTON STATE DEPARTMENT OF  
**NATURAL RESOURCES**  
WASHINGTON GEOLOGICAL SURVEY



# GEOLOGIC MAP OF THE COLOCKUM PASS SE 7.5-MINUTE QUADRANGLE, KITITAS COUNTY, WASHINGTON

---

by Andrew J. Sadowski and Todd R. Lau

WASHINGTON  
GEOLOGICAL SURVEY  
Map Series 2022-05  
December 2022

*This geologic map was funded in part by  
the USGS National Cooperative Geologic  
Mapping Program, award no. G21AC10798*

*This publication has been subject to an iterative technical review  
process by at least one Survey geologist who is not an author.  
This publication has also been subject to an iterative  
review process with Survey editors and cartographers.*



WASHINGTON STATE DEPARTMENT OF  
**NATURAL RESOURCES**  
WASHINGTON GEOLOGICAL SURVEY

## DISCLAIMER

Neither the State of Washington, nor any agency thereof, nor any of their employees, makes any warranty, express or implied, or assumes any legal liability or responsibility for the accuracy, completeness, or usefulness of any information, apparatus, product, or process disclosed, or represents that its use would not infringe privately owned rights. Reference herein to any specific commercial product, process, or service by trade name, trademark, manufacturer, or otherwise, does not necessarily constitute or imply its endorsement, recommendation, or favoring by the State of Washington or any agency thereof. The views and opinions of authors expressed herein do not necessarily state or reflect those of the State of Washington or any agency thereof.

## INDEMNIFICATION

Research supported by the U.S. Geological Survey, National Cooperative Geologic Mapping Program, under USGS award number G21AC10798. The views and conclusions contained in this document are those of the authors and should not be interpreted as necessarily representing the official policies, either expressed or implied, of the U.S. Government.

## WASHINGTON STATE DEPARTMENT OF NATURAL RESOURCES

Hilary S. Franz—*Commissioner of Public Lands*

## WASHINGTON GEOLOGICAL SURVEY

Casey R. Hanell—*State Geologist*

Jessica L. Czajkowski—*Assistant State Geologist*

Ana Shafer—*Assistant State Geologist*

### Washington State Department of Natural Resources Washington Geological Survey

*Mailing Address:*

1111 Washington St SE

MS 47007

Olympia, WA 98504-7007

*Street Address:*

Natural Resources Bldg, Rm 148

1111 Washington St SE

Olympia, WA 98501

*Phone:* 360-902-1450

*Fax:* 360-902-1785

*Email:* [geology@dnr.wa.gov](mailto:geology@dnr.wa.gov)

*Website:* <http://www.dnr.wa.gov/geology>

*Publications and Maps:*

[www.dnr.wa.gov/programs-and-services/geology/](http://www.dnr.wa.gov/programs-and-services/geology/publications-and-data/publications-and-maps)

[publications-and-data/publications-and-maps](http://www.dnr.wa.gov/programs-and-services/geology/publications-and-data/publications-and-maps)

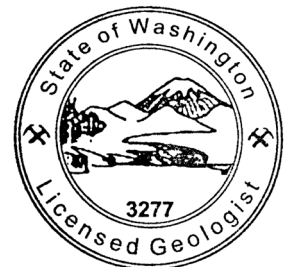


*Washington Geology Library Searchable Catalog:*

[www.dnr.wa.gov/programs-and-services/geology/](http://www.dnr.wa.gov/programs-and-services/geology/washington-geology-library)

[washington-geology-library](http://www.dnr.wa.gov/programs-and-services/geology/washington-geology-library)

*Suggested Citation:* Sadowski, A. J.; Lau, T. R., 2022, Geologic map of the Colockum Pass SE 7.5-minute quadrangle, Kittitas County, Washington: Washington Geological Survey Map Series 2022-05, 1 sheet, scale 1:24,000, 21 p. text. [[https://www.dnr.wa.gov/publications/ger\\_ms2022-05\\_geol\\_map\\_colockum\\_pass\\_se\\_24k.zip](https://www.dnr.wa.gov/publications/ger_ms2022-05_geol_map_colockum_pass_se_24k.zip)]



ANDREW JOHN SADOWSKI

*Andrew Sadowski*  
Dec 2022

# Contents

Introduction .....	1
Geologic Overview .....	2
Bedrock .....	2
Surficial Deposits .....	2
Tectonic Framework .....	2
Methods .....	2
Geologic Mapping .....	2
Data Collection and Analysis .....	3
Description of Map Units .....	3
Holocene to Pleistocene Nonglacial Deposits .....	3
Holocene to Pliocene(?) Alluvial Deposits .....	4
Tertiary Sedimentary and Volcanic Bedrock .....	5
Lithologies Depicted as Overlays .....	10
Mass Wasting (overlay mw) .....	10
Quaternary Loess (overlay Ql) .....	10
Miocene Hyaloclastite (overlay hy) .....	10
Summary of Geologic Structures .....	10
Geologic Structures Near Whiskey Ridge .....	11
Northerly Striking Faults (NSFs) .....	11
Discussion of Geophysics .....	11
Age of Faulting .....	13
Recommendations for Future Research .....	13
Acknowledgments .....	13
Author Contributions .....	13
References .....	13
Appendix A. Geophysics .....	17
Appendix B. Geochemistry .....	18
Appendix C. Geochronology .....	19

## TABLES

**Table 1.** Main characteristics of the units of the Columbia River Basalt Group (CRBG) in the Colockum Pass SE 7.5-minute quadrangle, northern Kittitas Valley .....8

**Table C1.** Detrital zircon maximum constraining ages from age sites GD3 and GD4.....20

## MAP SHEET

Geologic Map of the Colockum Pass SE 7.5-minute Quadrangle, Kittitas County, Washington

**Figure M1.** Geophysical interpretation for the map area



---

# Geologic Map of the Colockum Pass SE 7.5-minute Quadrangle, Kittitas County, Washington

by Andrew J. Sadowski<sup>1</sup> and Todd R. Lau<sup>1</sup>

<sup>1</sup> Washington Geological Survey  
1111 Washington St SE  
MS 47007  
Olympia, WA 98504-7007

## ABSTRACT

New geological and geophysical investigations of the Colockum Pass SE quadrangle refine Columbia River Basalt Group stratigraphy and characterize geologic structures in northeastern Kittitas Valley. New whole rock geochemistry from 169 locations builds upon existing magnetostratigraphy and locally refines the chemostratigraphic framework of the Grande Ronde Basalt (GRB) of the Columbia River Basalt Group, particularly for the Sentinel Bluffs Member. Flat-lying stratigraphy in the north—mostly composed of subunits of Sentinel Bluffs—becomes progressively tilted southward toward the range front as a result of faulting and folding. Interbeds of the sedimentary Coleman member are less common in the map area compared to quadrangles farther west, which suggests the unit's depositional center was farther west.

We identify oblique-slip and reverse faults and fault-related folds, including several northwest- through west-trending anticlines, synclines, and monoclines. We map a long, northwest-striking fault with an associated linear magnetic anomaly located southwest of a feature informally named “Whiskey ridge.” The Whiskey ridge fault continues beyond the western and southern edges of the map area. We also identify fault scarps in Quaternary deposits related to this structure that have various lengths and amounts of offset. Lastly, we map several short, northerly striking faults with small offsets that exhibit conspicuous scarps through Miocene bedrock.

Geophysical modeling of gravity and aeromagnetic data suggests laterally abrupt thickness changes in basaltic units. These thickness changes may be related to a period of syn-eruptive development of local accommodation space perhaps adjacent to growing folds.

## INTRODUCTION

The Colockum Pass SE 7.5-minute quadrangle (herein also referred to as “the map area”) is located in eastern Kittitas County in central Washington State. The map area covers the eastern and northeastern sectors of Kittitas Valley, which is located east of the Cascade Range on the western edge of the Columbia Basin. The map area is generally accessible with several gravel and dirt roads extending into the deep canyons, up hills, and along ridgelines.

Kittitas Valley is a northwest–southeast trending structural basin bound by anticlinal ridges in the south (Smith, 1903a, 1903b; Schuster, 1994) and monoclinical ridges in the north (Tabor and others, 1982; Sadowski and others, 2020, 2021). Elevation in the map area ranges from ~1,900 ft in the west to greater than 5,000 ft in the north. Several south- through west-flowing creeks drain deep canyons in the map area. For example, creeks in the west, such as Cooke Creek, drain to the south, whereas creeks in the east, such as Whiskey Jim creek, drain to the west, and creeks in between drain more to the southwest. These changes in drainage patterns are related to changes in the range front geometry and likely reflect associations with nearby geologic structures.

The range front of Kittitas Valley in the map area generally trends northwest. Northeast of the North Branch canal, we note a conspicuous, northwest-trending ridge between Caribou and Park Creeks, and we use the informal name “Whiskey ridge” for this feature. Whiskey ridge topographically separates the main portion of Kittitas Valley to the southwest from a smaller, elevated valley to the northeast and south of Spring Gulch.

Our 1:24,000-scale geologic mapping aims to improve understanding of the geologic history of Washington, characterize geologic hazards (earthquakes, landslides, debris flows), and locate natural resources (groundwater, aggregate). It builds upon prior geologic mapping at 1:100,000-scale (Waite, 1979; Tabor and others, 1982), nearby 1:24,000-scale mapping (Sadowski and others, 2020, 2021), and several partially overlapping, unpublished 1:12,000-scale geologic maps of Bentley and Powell from the early 1980s. Of those unpublished 1:12,000-geologic maps, three cover the southern third of the map area, and we partially adopted linework from those maps with some modification on our map, but we did not adopt the outdated unit classifications.



Our work is part of a multi-year geologic mapping project to characterize active faults in the region and better understand how the Yakima fold and thrust belt (YFTB) may transfer strain across the Cascade Range. In this map area we continued mapping structures that project southeastward from the adjacent map area of Sadowski and others (2021). The new mapping we present will assist in geologic hazard assessment, geotechnical engineering, groundwater hydrology, earth resource management, academic research, and investigations for growth management planning.

## GEOLOGIC OVERVIEW

### Bedrock

The oldest rocks exposed in the map area are basaltic andesite of the Miocene Grande Ronde Basalt (GRB) of the Columbia River Basalt Group (CRBG), a continental flood basalt province (Reidel and Tolan, 2013). Roughly 95 percent of the CRBG erupted rapidly between 16.7 and 15.9 Ma (Kasbohm and Schoene, 2018). The GRB constitutes about 72 percent of the CRBG formations by volume (Reidel and others, 2013a). The oldest exposed CRBG member in the map area is the Grouse Creek member in the northwest portion of the map. The youngest exposed CRBG member in the map area is the Wanapum Basalt in the southeastern corner of the map.

Volcaniclastic and feldspathic sedimentary rocks of the Ellensburg Formation unconformably overlie, interfinger, and underlie the CRBG (Schmincke, 1964, 1967; Smith, 1988a,b). The two general sources for these sedimentary rock types are recognized as (1) the ancestral Cascade Range that provided volcaniclastic detritus to the ancestral Columbia Basin, and (2) ancient rivers of the inland Pacific Northwest (such as the ancestral Columbia River) that provided feldspathic and micaceous material to the ancestral basin from distal sources (Schmincke, 1964, 1967; Smith 1988a,b). The Coleman member (Bentley, 1977) and Vantage member are mappable intervals within the Ellensburg Formation. The older Coleman member is a micaceous interbed that underlies the Sentinel Bluffs Member of the GRB, whereas the younger Vantage member is a pumiceous to micaceous interbed that overlies the Sentinel Bluffs and underlies the Wanapum Basalt.

### Surficial Deposits

Within the map area, Miocene bedrock is unconformably capped with Pliocene through Holocene nonglacial deposits (Porter, 1976; Waite, 1979; Sadowski and others 2020, 2021). Alluvium and alluvial fan deposits with various relative elevations, surface morphologies, and ages are present in the map area; these alluvial fans and terraces are generally composed of basalt cobbles.

Pleistocene eolian loess of the Palouse Formation is patchy and thin in northern Kittitas Valley compared to eastern Washington. The sediment source for loess was the wind-blown redistribution of fine-grained sand from ablation till, sandy to silty outwash, and (or) silt of slackwater deposits from cataclysmic floods related to continental glaciations (McDonald and Busacca, 1992). Landslide deposits and mass-wasting landforms are common and tend to mantle older units. These landforms are identified by their variable, hummocky surface morphologies. The

youngest surficial units in the valley (Qaf3 and younger)—and, where applicable, their channel networks—are extensively modified by agriculture, irrigation, and aggregate mining.

## Tectonic Framework

The map area lies within the modern backarc of the Cascadia subduction zone. During the Paleogene, non-marine Eocene sediments and volcanic rocks filled extensional and transtensional structural basins (Tabor and others, 1982; Johnson, 1985; Eddy and others, 2016, 2017; Donaghy and others, 2021) in the backarc. These continental basins were later filled and capped by voluminous Neogene lavas during the onset of Miocene compression and transpression, a stress regime that resulted from oblique subduction with steady, regional, clockwise rotation of the crust (Reidel and others, 1984; Wells and McCaffrey, 2013; Brocher and others, 2017). Global Positioning System (GPS) velocities reveal that ongoing north–northeast-directed shortening (McCaffrey and others, 2013; Wells and others, 1998) is accommodated by extensive, kilometer-scale, west- and northwest-striking, reverse-to-thrust faults and associated folds of the YFTB (Reidel and others, 2013b; Kelsey and others, 2017; Staisch and others, 2018a,b). The map area encompasses the northern extent of the YFTB from Kittitas Valley to the Wenatchee Mountains (Rosenmeier, 1968; Tabor and others, 1982).

## METHODS

### Geologic Mapping

We identified lithologic units from field observations in the summer and fall of 2021. We collected over 700 field data points using traditional geological field methods and digitally recorded them with Esri's ArcGIS Field Maps application. We reviewed prior geologic mapping at 1:100,000 scale (Waite, 1979; Tabor and others, 1982), three unpublished 1:12,000-scale field map sheets (written commun., by R. Bentley and J. Powell, 2013), recent aerial orthophotos, and elevation data from lidar (PSLC, 2011; WA DNR, 2014). We used lidar data to derive slope, hillshade images, and contours. We also note that there are multiple cross sections from unpublished mapping that are subparallel to our A–A' profile; however COVID-19 restrictions at Grant Public Utility District prevented us from viewing these materials prior to generating our cross section (see the Map Sheet).

We measured over 136 bedding attitudes, sedimentary structures, igneous foliations, joints, and shears. We compiled 41 of those 136 measurements with little to no modification from unpublished mapping (R. Bentley and J. Powell, affiliations, written commun., 2013) in the southern third of the map area. These compiled measurements are highlighted using a different color on the map sheet. Due to scale, not all measurements are shown on the map sheet but all are in the GIS data.

We describe flood basalt intraflow textures (physical volcanology), generally found in the following order (from bottom to top): hyaloclastites of pillow-palagonite breccias, basal colonnades, entablatures, internal vesicular zones, vesicular tops, and autobreccias (Reidel, 2015). The physical volcanology of the flows helps us assess the flow-by-flow stratigraphy and choose samples to analyze for whole-rock geochemistry that can be



compared to previous work (Reidel, 2005; Reidel and Tolan, 2013; Hammond, 2013; Sadowski and others, 2020, 2021) to elucidate chemostratigraphy. In CRBG rocks, planar orientations of flow foliation surfaces are measured on vesicular and colonnade tops. Similarly, the orientations of upright column sides in colonnade sections are also measured and analyzed stereographically using Stereonet 10.1.0 software (Allmendinger and others, 2012; Cardozo and Allmendinger, 2013) to determine cooling surfaces inferred to represent paleo-horizontal.

## Data Collection and Analysis

We reviewed multiple datasets to inform our mapping and subsurface understanding: well logs, boring records, water wells ( $n=25$ , all  $<850$  ft deep), geophysical data (gravity and aeromagnetism), geochemical analyses (major and trace elements using X-ray fluorescence only), petrographic analysis of thin sections, aerial photos, and lidar data.

## POTENTIAL-FIELDS GEOPHYSICAL METHODS

We collected 173 new gravity observations using a Scintrex model CG-6 gravimeter and combined these with 677 points from previous studies (Sadowski and others, 2020, 2021). Our methods for collecting gravity data are described in Appendix A. The gravity data are listed in the Data Supplement, and are viewable as an isostatic anomaly map on the Map Sheet (white contours on Figure M1A). We also collected gravity measurements outside of the map area to prevent introducing potentially spurious edge effects into our gravity results (Figure M1A). We also used aeromagnetic data from two surveys (Blakely and others, 2020a,b) to identify magnetic anomalies related to volcanic bedrock and highlight lineaments possibly related to faults or folds.

Forward modeling of the gravity and aeromagnetic potential-field data along Cross Section A–A' using GM-SYS (Geosoft, Inc.) helps constrain possible bedrock geometries in the subsurface. We present a geophysical model (Figure M1B) that we produce through an iterative process of adjusting model geometries to fit observations and interpretations from the map's geology and geophysics, which in turn informs the geologic cross section geometries and vice versa. Models that do not fit observed geophysical anomalies or do not honor geologic constraints are discarded. The resulting model we present is a plausible interpretation of the subsurface geology. We calibrate our modeling parameters for local geologic units with published rock properties (Staisch and others, 2018a,b), and with density and magnetic susceptibility measurements, including 145 measurements from previous studies (Sadowski and others, 2020, 2021) and 90 new measurements from this study.

## GEOCHEMISTRY

A total of 169 geochemistry samples of mostly basaltic andesite rocks from the map area were submitted for whole-rock geochemistry (X-ray fluorescence only) to the Peter Hooper GeoAnalytical Lab at Washington State University (WSU) (see Appendix B and Data Supplement). Geochemistry sites G001–G159 are in the map area, whereas sites G160–G169 are outside of the quadrangle to the north or east. We collected an additional 76 geochemical samples in and around the quadrangle map area to the south: the East Kittitas 7.5-minute quadrangle.

These 76 samples were also collected during the 2021 field season and inform the geology we present in this map, but are not formally published here. The data will be published in an upcoming publication for the East Kittitas map area.

We used the machine learning (ML) model developed by Dr. Ashley Steiner at the WSU Peter Hooper GeoAnalytical Lab to categorize GRB members, submembers, and formations using major and trace element geochemical data alone. The ML model does not consider stratigraphic context when making its classifications. Overall, the model does a better job distinguishing formation-level units from each other (for example, Wanapum versus Grande Ronde) than member-level or submember-level units from each other. For this reason, we relied less on the ML model for member-level and submember-level classifications compared to previous years. Instead, we plotted elemental variation diagrams ( $\text{TiO}_2$  vs  $\text{MgO}$ ,  $\text{TiO}_2$  vs  $\text{P}_2\text{O}_5$ , and amounts of Zr and Cr) and used stratigraphic understanding to determine the most reasonable member and submember classifications, especially when ML classifications had low confidence values.

## GEOCHRONOLOGY

We used U-Pb analysis of detrital zircons by Laser Ablation Inductively Coupled Plasma Mass Spectrometry to assess provenance and depositional age for sedimentary deposits (see Data Supplement). To do this, we sent approximately 7 kg of sample to ZirChron LLC for mineral separation. Zircon separates were analyzed by Vic Valencia and Jeff Vervoort at the Radiogenic Isotope and Geochronology Lab at WSU. Detailed methods can be found in Appendix C.

## DESCRIPTION OF MAP UNITS

### Holocene to Pleistocene Nonglacial Deposits

- |    |  |
|----|--|
| af | <b>Artificial fill (Holocene)</b> —Cobbles, pebbles, sand, and boulders; poorly sorted and unconsolidated; placed to elevate home sites, highways, railroads, or other infrastructure.   |
| ml | <b>Modified land (Holocene)</b> —Sand- through boulder-sized material, redistributed to modify topography for industrial, agricultural, and residential uses, including but not limited to gravel pits, rock quarries, aggregate mines, excavator training locations, and home sites.  |
| Qp | <b>Peat (Holocene to Pleistocene)</b> —Organic and organic-rich sediment; includes peat, gyttja, muck, silt, and clay; typically in closed depressions; mapped in natural or man-made wetlands, bog areas, and ephemeral water bodies; also mapped from assessing black-and-white aerial photos where black to dark gray ephemeral ponds and water bodies were not mapped in the published base map. Man-made water bodies likely contain smaller (or no) peat deposits than older, natural features. The thickness of most peat deposits is largely unassessed but presumed to be less than 10 m. Small peat deposits are scattered throughout the map area, typically within |

alluvium, and are related to ponding of stagnant water or agricultural activities.

**Qls** **Landslide deposits (Holocene to Pleistocene)**—Clastic aggregate and scree; medium brown to light yellowish brown, weathering is typically mild or moderate; generally loose and poorly consolidated; clay to boulder-sized clasts; angular to subangular; unsorted, typically matrix supported, and less commonly clast supported near talus piles; unstratified and structureless; unit contains rubble of sand, silt, clay, cobbles, pebbles, boulders, and diamicton of mostly basalt clasts and sometimes fine sand derived from nearby sedimentary units or soils; deposit thicknesses are less than 30 m and typically less than 15 m; unit is generally found in the uplands along steep, canyon slopes or where associated with sedimentary bedrock units, for example near the mouth of Caribou Creek canyon (north of Secret Canyon Road). Several landslides along the steep, southern wall of Caribou Creek canyon (south of Secret Canyon Road) may be more colluvial in origin—or scree-like—and are associated with alluvial fans at their bases (unit Qaf). A mass-wasting overlay (mw) is used to delineate landforms with landslide-like characteristics (such as hummocky topography) that are difficult to confidently characterize as landslide deposits. These overlays suggest places where evidence for landslide deposits is inconclusive and mass wasting may be related to other processes (such as soil creep and solifluction). Landslides and mass-wasting overlays are mapped primarily based on landform morphology. Absence of a mapped landslide or mass-wasting overlay does not indicate the absence of landslide hazard; site-specific investigations—and not this mapping alone—are recommended to further assess identified landslide hazards. Ages and recurrences of deposits are unknown.

### Holocene to Pliocene(?) Alluvial Deposits

Stream channel and stream flood (overbank) deposits and terraces. Deposits include pebbles, cobbles, sand, silt, clay, peat, and boulders, all in varying amounts and thicknesses. Colors range from light tannish gray to medium brown. The deposits are fresh to mildly weathered, and are not compacted or cemented. The clasts are typically cobbles with sand and gravel, well rounded, moderately to well sorted, and mostly composed of basalt.

**Qa** **Alluvium (Holocene)**—Stream channel deposits on active flood plain, depositional environment is the active flood plain; unit is narrowly distributed throughout low elevations of the map area and these deposits commonly flank creeks; areas of this unit have been heavily modified by agricultural cultivation and have map patterns that reflect such modification, such as sharp angles. The age of unit Qa is unknown and we infer ongoing alluvial deposition on the surfaces of the unit.

**Qia**

**Intermediate-aged alluvium (Holocene to Pleistocene)**—Stream flood (overbank) and old channel deposits near active flood plains, where ongoing alluvial deposition from overland flow is possible but less clear compared to unit Qa; unit is limited to the western half of the map area; surfaces of unit Qia are slightly elevated relative to the surfaces of unit Qa. Unit Qia is commonly indistinguishable from alluvial fan unit Qaf1 based on lithology and height relative to unit Qa. However, unit Qia tends to be found (1) closer to unit Qa than unit Qaf1, and (2) at slightly lower elevations than unit Qaf1. Unit Qia is also inferred to be slightly younger than Qaf1 because of these elevation differences. Note that older alluvium, unit Qoa, was not mapped here but is located in this region farther west of the map area (Sadowski and others, 2020).

We performed U-Pb analysis of detrital zircons at age site GD01 (located ~10 m above the active stream channel) to determine the age of the deposit (see Data Supplement and Appendix C). We initially thought the sample might belong to a different, older bedrock unit, but the sample yielded a Quaternary age and we now suspect that the sample belongs to unit Qia.

**Qaf**

**Alluvial fan deposits (Holocene to Pliocene?)**—Sand and gravel deposited in alluvial fans and other relict debris flow deposits; colors range from various shades of brown to brownish medium gray; weathering rinds vary from less than 1 mm up to 1 cm; uncompacted to poorly consolidated; silt- to boulder-sized clasts; angular to subrounded; unsorted; clast composition is generally basalt of the CRBG and depends on the composition of bedrock from which the unit is derived; unit thickness is generally less than 15 m but varies with age, where older units tend to be thicker.

Unit is subdivided and numbered from 1 (lowest and youngest) to 4 (highest and oldest) based on relative elevation above the modern stream level and differences in surface morphologies. A site from unit Qaf3 (Sadowski and others, 2020) yields a luminescence age of  $468.9 \pm 54.5$  ka. Units Qaf1 and Qaf2 are inferred to be younger, and unit Qaf4 is inferred to be older than that age. Older surfaces are smoother and more deeply incised, whereas younger surfaces are inset and rougher but less incised; weathering rinds are <1 mm on unit Qaf1, about 1 mm on units Qaf2 and Qaf3, and >1 mm on unit Qaf4. Loess patterns are common on older surfaces. Fault escarpments are common and sharp within units Qaf3 and Qaf4. Silicic caliche (hardpan) is more common in older units Qaf3 and Qaf4. Surfaces of unit Qaf3 to the east of Park Creek are marginally inset (<3 ft elevation difference) against surfaces that exhibit similar roughnesses, depths of incision, and amounts of dissection. These similar-looking Qaf3 surfaces are also slightly more elevated eastward (<3 ft elevation change) (see both sides of 'Geologic boundary' symbol near southern map boundary on Map Sheet). Therefore, we interpret unit

Qaf3 to be progressively slightly older—but not old enough to be unit Qaf4—to the east of Park Creek. Here, unit Qaf3 is also likely locally derived from the shallowly concealed sandstone of the Vantage Member (unit M<sub>Cev</sub>). Numerous generations of alluvial fans are exposed in the western and southern parts of the map area.

## Tertiary Sedimentary and Volcanic Bedrock

### SEDIMENTARY ROCKS OF THE ELLENSBURG FORMATION

**M<sub>Ce</sub> Ellensburg Formation, undivided (Miocene)**—Feldsarenite of volcanoclastic to lacustrine or fluvial origin underlying(?), intercalated with, and overlying rocks of the CRBG; light to medium brown to light to medium gray; mildly to strongly weathered; moderately indurated; where interbedded in the CRBG, unit is generally fine- to coarse-grained sandstone, where unconformably overlying the CRBG—upper Ellensburg Formation—unit may be locally conglomeratic or partly laharic in the southwestern part of the map area; subrounded or subangular; well to moderately sorted; grain supported; sand composition includes quartz (20–35%), feldspar (plagioclase 10–20%, potassium feldspar 5–15%), and lithic fragments (3–10%) with varying abundances of white to clear mica (0–30%, muscovite); generally less than 90 m thick; interbed exposures are thin, discontinuous, and poorly exposed in the GRB along cliffs and topographic saddles and benches, whereas exposures of upper Ellensburg Formation that unconformably overlie the CRBG can form well-exposed roadcuts with lighter color tones. Unit is also inferred in areas where we lack outcrop but where there is colluvial float or other geomorphic indicators of a sedimentary interbed. Thin (<1 ft), siliceous caliche layers are common and discontinuous in the near surface (<3 m below modern ground surface). Unit locally and unconformably onlaps the Wanapum Basalt in the southwestern part of the map area. The upper portions of the unit commonly lack white mica, whereas older members interbedded with basalt commonly have white mica in varying amounts. Variations in mica abundance likely reflect changes in provenance, where greater mica abundances may be correlated with sourcing from more distal locations such as northeast Washington or northern Idaho. Unit M<sub>Ce</sub> is divided into other named sedimentary units based on stratigraphic relationship to CRBG units (such as Wanapum, Grande Ronde, or Sentinel Bluffs units):

**M<sub>Cev</sub> Vantage member of the Ellensburg Formation (Miocene)**—Micaceous sandstone and siltstone; light brownish gray to light gray or white, moderately to strongly

weathered; mildly to moderately indurated, mildly cemented; subangular; fine to coarse grained; commonly well sorted, grain supported; sand composition is variable and includes quartz (30–60%), potassium feldspar (<30%), plagioclase feldspar (<10%), and lithic fragments (<5%); lithic fragments are generally quartzite or basalt; sand commonly contains white to clear muscovite (5–30%, 0.1–0.5 mm, max 1.5 mm). White pumice fragments and basalt-derived lithic fragments that typified this unit in the adjacent map area (Sadowski and others, 2021) are less common in the current map area and may have been incorporated into the matrix of this unit. Unit thickness is greater than 30 m. The unit is located in the south-central portion of the map area, and is more common in our map area compared to adjacent map areas farther west (Sadowski and others, 2021). Exposures of clastic aggregate with matrix-supported angular basalt clasts were mapped by Tabor and others (1982) as unit M<sub>Cev</sub> near the bend in Venture Road and along the range front between Caribou and Park creeks (Tabor and others, 1982), but we disagree with their interpretation and instead map alluvial deposits here (alternatively, this could be fault-related breccia or colluvium). The paleogeography of this unit is presumed to be continental paleotopographic lows that contain water bodies (rivers or lakes?) with a fluvial depositional environment that may have incorporated distally sourced micaceous sedimentary material and reworked near-source pumiceous material (pyroclastic or volcanoclastic?) from the ancestral Cascade Mountains. The unit unconformably overlies the GRB in and around Kittitas Valley and resides between the underlying GRB Formation—where the top of GRB is the basalt of Museum of the Sentinel Bluffs Member, unit M<sub>Vgsm</sub>—and the overlying Wanapum Basalt Formation. Reference localities include sparse outcrops near Western WA Operating Engineers training areas located to the north of Vantage Highway and east of Park Creek.

**M<sub>Cec</sub> Coleman member of the Ellensburg Formation, undivided (Miocene)**—Sandstone and siltstone underlying the Sentinel Bluffs Member of the CRBG; medium brown to light gray; generally micaceous, fine- to medium-grained sandstone; inferred to be less than 60 m thick. Unit is discontinuous and poorly exposed at mid-to-low elevations in the map area, and likely



pinches out eastward at Little Caribou Creek. This may suggest that the Coleman member's depositional center is farther west outside the map. We also interpret its depositional environment to be a Miocene fluvial and (or) lacustrine setting. Unit is discontinuously mapped in conspicuous topographic saddles below the basalt of McCoy Canyon (unit **Mv<sub>gsmc</sub>**) of the Sentinel Bluffs Member of the GRB. Hyaloclastites associated with GRB flows near unit **Mc<sub>ec</sub>** are less common in the map area compared to quadrangles to the west. Landslides are common downslope of the Coleman member. At depth in Kittitas Valley, the Coleman member may form an aquifer or an aquitard. In the latter case, if volcanoclastic content (ash weathering to clay) is abundant, these weathering products could perch groundwater resources into the overlying basalts. The unit was informally named by Bentley (1977) near Coleman Canyon of northern Kittitas Valley and mapped by Hammond (2013) as far south as the Naches River area. It is equivalent to the farther north Rock Island member of Hoyt (1961), the Douglas Creek member of Ebinghaus and others (2015), and the Rock Island arkosic sands of Schmincke (1967). Unit **Mc<sub>ec</sub>** is presented as “undivided” because available exposures in the map area proved insufficient for recognition of grain size subdivisions (similar to those reported outside the map area by Sadowski and others, 2020, 2021).

## VOLCANIC ROCKS OF THE COLUMBIA RIVER BASALT GROUP (CRBG)

**Mv<sub>w</sub>** **Wanapum Basalt (Miocene)**—Basalt; dark gray to grayish brown; well indurated; mostly microporphyritic to weakly glomerocrystic, commonly with groundmass crystals larger than 1.0 mm and less commonly aphyric than GRB units; euhedral; groundmass textures are microcrystalline, equigranular to seriate, and plagioclase microlite laths are unoriented (pilotaxitic more than trachytic); in the map area we infer the presence of the unit where moderate-relief landforms are found stratigraphically above unit **Mc<sub>ev</sub>**. Based on nearby geochemical data from adjacent map areas (Sadowski and others, 2021), the unit in this map area is likely composed of the Frenchman Springs Member and (or) the Priest Rapids Member. Unit thickness is less than 61 m. Unit is found in the southwestern corner of the map area. There, our geophysical modeling of aeromagnetic anomalies suggests dense rocks with reverse magnetic remanence in the shallow subsurface. The Priest Rapids Member (unit **Mv<sub>wp</sub>** in Sadowski and others, 2021) is nearby and also has reverse magnetic remanence. Therefore, in the map area, unit **Mv<sub>w</sub>** is

**Mv<sub>g</sub>**

possibly the Priest Rapids compositional type but we lack the outcrops and geochemical samples to fully support this interpretation. The unit unconformably overlies the Vantage member (unit **Mc<sub>ev</sub>**), and unit **Mc<sub>e</sub>** unconformably onlaps onto unit **Mv<sub>w</sub>**.

**Grande Ronde Basalt (GRB), undivided (Miocene) (cross section only)**—Basaltic andesite, described in detail in the following units. Generally, GRB rocks in hand specimen are very dark to medium gray where fresh, dark to medium brown where weathered, and dense; in thin section they show euhedral laths of plagioclase microlites intermeshed in an irregular and unoriented microcrystalline groundmass texture (pilotaxitic or felty). The map area is primarily composed of GRB with thin, sedimentary interbeds.

GRB members were previously mapped using a portable fluxgate magnetometer and categorized into four polarity chronostratigraphic units, also known as magnetostratigraphic units (MSU). These magnetostratigraphic units of the GRB are from oldest to youngest: reverse magnetic polarity 1 (R1 MSU), normal magnetic polarity 1 (N1 MSU), reverse magnetic polarity 2 (R2 MSU), and normal magnetic polarity 2 (N2 MSU) (Tabor and others, 1982; Reidel and Tolan, 2013; Hammond, 2013). In the map area, R1 and N1 MSU have not been observed and we subdivide R2 and N2 MSU further into chemostratigraphic subunits where geochemistry data is available (see Table 1 and Data Supplement). Stratigraphic relationships and geochemical variation diagrams (especially TiO<sub>2</sub> vs. MgO and TiO<sub>2</sub> vs. P<sub>2</sub>O<sub>5</sub>) from Hammond (2013) and Sadowski and others (2020, 2021) aid unit classification. On the Map Sheet we distinguish individual lava flows of a single geochemically distinct unit, where vesicular tops and (or) topographic slope breaks indicate flow boundaries. These boundaries are symbolized as dark gray lines (see ‘Geologic Boundary’ in the map legend). Unit **Mv<sub>g</sub>** is inferred where geochemistry was unavailable, outcrops were absent, inference for a particular subunit was overly speculative, or units were grouped at depth in cross section (for example, Grouse Creek (R2 MSU) and older GRB units).

Stratigraphy in our map area is remarkably similar to the stratigraphy of Hammond (2013, see figure 4 therein) in the Naches River area and to the westward adjacent mapping by Sadowski and others (2021). Without the base exposed, we map the GRB with a thickness of at least ~400 m. CRBG thickness is interpreted from a nearby hydrocarbon exploration borehole: the Shell BISSA 1-29 borehole (API# 046037-00006) is located ~1.4 miles (~2.25 km) east of the map area and more than 5 miles (8 km) from the cross section and geophysical model. The borehole has about 4,600 ft (~1,400 m) of GRB interpreted, assuming no faulting through the borehole (Wilson and others, 2008; Czajkowski and others, 2012). However, there may be a fault downhole through the Wapshilla

Ridge Member (part of the R2 MSU; S. Reidel, WSU Tri-Cities, written commun., 2020).

**Mvgs Sentinel Bluffs Member, undivided (Miocene)**—Basaltic andesite; aphyric; the map area contains four subunits, from oldest to youngest: basalts of McCoy Canyon, Spokane Falls, Stember Creek, and Museum, where the middle two subunits are portions of the “Cohassett flow” (Reidel, 2005) that may be intermingling compositional types and may locally exhibit an internal vesicular zone (IVZ) related to “flow inflation” (McMillan and others, 1989; Reidel, 2015). Where present, the IVZ may obscure the locations of vesicular flow tops identified from surface mapping of physical volcanology characteristics, because vesicular flow tops and the IVZ look similar. Where geochemical results are available (See Table 1 and Data Supplement), we use cross comparisons of geochemical variation diagrams ( $\text{TiO}_2$  vs.  $\text{MgO}$ ,  $\text{TiO}_2$  vs.  $\text{P}_2\text{O}_5$ , Zr, and Cr, for example) and stratigraphic relationships to classify flows geochemically. This is especially useful where elemental compositional fields partially overlap for the middle-to-upper subunits on  $\text{TiO}_2$  vs.  $\text{MgO}$  diagrams but not necessarily on  $\text{TiO}_2$  vs.  $\text{P}_2\text{O}_5$  diagrams. Cumulatively, the Sentinel Bluffs Member is at least ~152 m thick, and its sub-units are common throughout the map area. The unit was mapped as GRB N2 MSU (Tabor and others, 1982). Unit **Mvgs** is mapped as undivided (“grouped”), where geochemical results are unavailable to divide exposures into subunits and where reasonable interpolations are made using nearby stratigraphic relationships. The geochemical compositional ranges of all subunits of unit **Mvgs**—that is the elemental composition of the Sentinel Bluffs Member as a whole—generally are:  $\text{TiO}_2$ : ~1.7–2.0 wt. %,  $\text{MgO}$ : ~3.8–5.5 wt. %,  $\text{P}_2\text{O}_5$ : ~0.24–0.36 wt. %, Zr: ~149–178 ppm. With available whole-rock geochemistry (see Data Supplement), the Sentinel Bluffs Member is subdivided into:

**Mvgsm Basalt of Museum (Miocene)**—Fine-grained basaltic andesite with groundmass crystals ranging in size from 0.05 to 0.6 mm and very rare phenocrysts of plagioclase up to 3.5 mm in size; most commonly aphyric; groundmass textures are microcrystalline, mostly equigranular (rarely seriate), and pilotaxitic (unoriented); see approximate

ranges for elemental compositions in Table 1. Other contents include mafic minerals (20–40%, 0.1–0.5 mm, mostly clinopyroxene) and devitrified glass that is absent or rare. From map patterns, unit thickness is greater than 30 m. The upper contact is generally poorly exposed. For example, the upper contact of the unit with the Vantage Member is exposed east of Park Creek on Western Washington Operating Engineers property in the southwestern map area. At depth, unit thickness in the BISSA well is ~60 m (S. Reidel, WSU Tri-Cities, written commun., 2020). Unit contains at least two flows with colonnades, entablatures, and vesicular tops that are all well developed. Unit is widespread and found along the lower portions of the range front and at high elevations to the north and east. Unpublished mapping by Bentley and Powell in the early 1980s labels this unit as Tmz (Museum), Tor (Ortley Rocky Coulee), or Trc (Rocky Coulee), but recent refinement of GRB stratigraphy (Reidel, 2005; Reidel and Tolan, 2013) lumped these compositional types together as the basalt of Museum, which we adhere to.

**Mvgssc Basalt of Stember Creek (Miocene)**—Fine-grained basaltic andesite with groundmass crystals ranging in size from 0.05 to 0.4 mm and very rare phenocrysts of plagioclase as large as 1.6 mm; most commonly aphyric; groundmass textures are microcrystalline, seriate more than equigranular, and pilotaxitic (unoriented); see approximate ranges for elemental compositions in Table 1. Unit **Mvgssc** generally has diagnostically lower zirconium values compared to other sub-units of the Sentinel Bluffs Member, and zirconium values are particularly effective for distinguishing unit **Mvgssc** from unit **Mvgssf**, especially where stratigraphic relationships are less straightforward. Other

**Table 1.** Main characteristics of the units of the Columbia River Basalt Group (CRBG) in the Colockum Pass SE 7.5-minute quadrangle, northern Kittitas Valley. See text and Data Supplement Table DS01 for more details. Mafic mineral abbreviations: cpx = clinopyroxene, ol = olivine, opx = orthopyroxene. MSU, magnetostratigraphic units. Analyte uncertainties: TiO<sub>2</sub> (±0.012 wt. %), MgO (±0.073 wt. %), P<sub>2</sub>O<sub>5</sub> (±0.003 wt. %), Zr (±5.7 ppm), Cr (±2.9 ppm).

Unit label		Mvgsm	Mvgssc	Mvgssf	Mvgsmc	Mvgo	Mvgg
Unit name		Basalt of Museum	Basalt of Stember Creek	Basalt of Spokane Falls	Basalt of McCoy Canyon	Ortley Member	Grouse Creek Member
Unit thickness (m)		>30	<60	<60	>60	150	>45
Texture		aphyric, aphanitic	aphyric, aphanitic	aphyric, aphanitic	aphyric, aphanitic	aphyric, aphanitic, diktytaxitic	aphyric, aphanitic
Crystal size (mm)		0.05–0.6, max 3.5 mm	0.05–0.4, max 1.6 mm	0.1–0.4, max 1.2 mm	0.1–0.5, max 1.2 mm	<1.0	<1.5
Mafic minerals (% , size, abundance)		20–40%, 0.1–0.5 mm, mostly cpx	<30%, ~0.05–0.35 mm, mostly cpx	20–40%, 0.1–0.4 mm, mostly cpx	5–40%, 0.05–0.5 mm, mostly cpx	no data	no data
Approximate ranges for whole rock elemental compositions (XRF)	TiO <sub>2</sub> (wt. %)	1.7–1.8	1.7–1.8	1.77–1.88	1.87–1.95	1.85–1.95	1.84
	MgO (wt. %)	4.0–5.0	4.2–5.5	4.2–5.0	4.3–5.0	3.0–3.7	4.11
	P <sub>2</sub> O <sub>5</sub> (wt. %)	0.32–0.34	0.24–0.28	0.30–0.36	0.27–0.31	0.30–0.33	0.294
	Zr (ppm)	161–178	149–159	159–170	157–166	177–202	167
	Cr (ppm)	37–44, avg. ~40	45–56, avg. ~50	34–48, avg. ~42	19–37, avg. ~23	5–8	17
Magnetostratigraphy		Normal (N2 MSU)	Normal (N2 MSU)	Normal (N2 MSU)	Normal (N2 MSU)	Normal (N2 MSU)	Reverse (R2 MSU)
Notes		Top of Sentinel Bluffs Member locally. Upper contact not well exposed	Interfingers with Spokane Falls member	Interfingers with and inflated the Stember Creek member	Bottom of Sentinel Bluffs Member locally.	Unit is invasive to the west of the map area and contains peperitic hyaloclastite there.	Data from one sample. Bottom is not exposed. Thickness could be > 300 m.

contents include mafic minerals (<30%, 0.05–0.35 mm, mostly clinopyroxene) and some devitrified glass (0–15%). From map patterns, unit thickness is less than ~60 m, and thins and pinches out to the northeast. Unit is not observed in the BISSA well at depth (S. Reidel, WSU Tri-Cities, written commun., 2020). Unit contains at least two flows with common basal colonnade, interior entablature, and vesicular flow top, with uncommon hyaloclastite horizons. Unit consistently overlies flows with Spokane Falls-type compositions in the map area, and—as depicted in Reidel (2005, 2015)—may also inter-finger with flows of the Spokane Falls-compositional type in the

northeast map area. Unit is well exposed east of Cooke Canyon, at middle and higher elevations, and is as common as the basalt of Spokane Falls. Unpublished mapping by Bentley and Powell in the early 1980s labels this unit as Toc (Ortley Cohassett?) or Tch (Chinahat/Cohassett?).

Mvgssf

**Basalt of Spokane Falls (Miocene)**—Fine-grained basaltic andesite with groundmass crystals ranging in size from 0.1 to 0.4 mm and very rare phenocrysts of plagioclase as large as 1.2 mm; most commonly aphyric; groundmass textures are microcrystalline, range from seriate to equigranular, and pilotaxitic (unoriented); see approximate



ranges for elemental compositions in Table 1. Unit **Mvgssf** has diagnostically higher zirconium values than unit **Mvgssc**, but unit **Mvgssf** can be challenging to distinguish from other subunits of the Sentinel Bluffs Member that have similar geochemistry. Other contents include mafic minerals (20–40%, 0.1–0.4 mm, mostly clinopyroxene), opaque minerals (~40%), and some devitrified glass (0–20%). From map patterns, unit thickness is less than 60 m and may pinch out to the north-northeast, whereas at depth, unit thickness in the BISSA well is ~60 m (S. Reidel, WSU Tri-Cities, written commun., 2020). Unit contains at least two flows and consistently underlies rocks with Stember Creek-type compositions (possibly near IVZ), and—like as depicted in Reidel (2005, 2015)—may interfinger with rocks with Stember Creek-type compositions. Unit exhibits common basal colonnade, interior entablature, and vesicular flow top with rare hyaloclastite horizons. Unit is found commonly in middle elevations of the northern range front, higher elevations to the north, and low elevations in canyon bottoms of Park and Trail creeks. Unpublished mapping by Bentley and Powell in the early 1980s labels this unit as Toj (Ortley Jim?) or Tbt (Bingen unknown designation?).

**Mvgsmc Basalt of McCoy Canyon (Miocene)**—Fine-grained basaltic andesite with groundmass crystals ranging in size from ~0.1 to 0.5 mm and very rare phenocrysts of plagioclase as large as 1.2 mm; most commonly aphyric; groundmass texture is microcrystalline, equigranular, pilotaxitic (unoriented), and uncommonly microvesicular; see approximate ranges for elemental compositions in Table 1. Includes mafic minerals (5–40%, 0.05–0.5 mm, mostly clinopyroxene) and some devitrified glass (0–10%). From map patterns, unit thickness is a least

60 m thick, whereas at depth, unit thickness in the BISSA well is at least ~90 m thick (S. Reidel, WSU Tri-Cities, written commun., 2020). Unit contains two or three flows and forms well-developed entablature with short basal colonnade, and commonly has a vesicular flow top and hyaloclastite horizons near its base. Unit overlies the Coleman member of the Ellensburg Formation (unit **Mcce**) in the northwest map area. Unpublished mapping by Bentley and Powell in the early 1980s labels this unit as Tbb (Bingen Bumping Hollow?) or Tmc (McCoy).

**Mvgo**

**Ortley member (Miocene)**—Fine- to medium-grained basaltic andesite with groundmass crystals up to 1 mm in size; most commonly aphyric; groundmass texture is weakly microporphyritic, pilotaxitic (unoriented), and mildly microvesicular (diktytaxitic). Elemental compositions are similar to the underlying Grouse Creek member such that compositional fields may overlap. See approximate ranges for elemental compositions in Table 1. From map patterns, unit thickness is ~150 m thick, whereas at depth, unit thickness in the BISSA well is ~230 m (S. Reidel, WSU Tri-Cities, written commun., 2020). Unit is widespread at the lower elevations of the deep canyons of Caribou Creek (Secret Canyon Rd) and Park Creek. Unit contains at least two to four flows and commonly forms well-developed vesicular flow tops, entablatures, and palagonitic hyaloclastites, whereas basal colonnades are rare. The Ortley member overlies the Grouse Creek member (unit **Mvgg**) at geochemistry site G001 in Cooke Canyon, and is overlain by the sedimentary Coleman member (unit **Mcce**). Unit is part of the N2 MSU and represents the base of N2 MSU in the map area. Compared to this unit in westward adjacent areas (Sadowski and others, 2021), peperitic hyaloclastite that indicates invasion of lava into un lithified sediment is not identified in this map area. Hyaloclastites and pillow breccias are also less common in our map area compared to western areas (Coleman Canyon and westward), and the scarcity of these three features may suggest that unit **Mvgo** is less invasive in the map area. Unpublished mapping by Bentley and Powell in the early 1980s labels this unit as Tbp

(Bingen unknown designation?) or Tbw  
(Bingen unknown designation?).

Mv<sub>gg</sub>

**Grouse Creek member (Miocene)**—Medium- to fine-grained basaltic andesite with groundmass crystals less than 1.5 mm in size; aphyric; groundmass texture is generally pilotaxitic (unoriented) with groundmass crystal sizes slightly greater than those of unit Mv<sub>gs</sub>; see elemental compositions in Table 1. Base of unit is not observed. From map patterns, unit thickness in the map area is greater than 45 m but may be considerably thicker, as suggested by a 180+ m section west of the map area (Sadowski and others, 2021), whereas at depth, unit thickness in the BISSA well is ~90 m (S. Reidel, WSU Tri-Cities, written commun., 2020). Unit contains at least one flow and forms common fanning entablatures, autobreccias, and some platy entablature, but vesicular tops are thin, poorly developed to absent, and we do not observe colonnades in this unit. Unit is found in the map area only in Cooke Canyon. Unit commonly contains hyaloclastite outside the map area but lacks hyaloclastite exposures in the map area. The closest hyaloclastite to unit Mv<sub>gg</sub> is in the overlying Ortley member (unit Mv<sub>go</sub>) near Ortley's basal contact. Unit was mapped as the Howard Creek invasive flow by Rosenmeier (1968), GRB MSU R2 by Tabor and others (1982), the Meeks Table flow by Swanson (1976, 1978), Bentley (1977), and Hammond (2013). Unit represents the top of the R2 MSU in the map area.

## LITHOLOGIES DEPICTED AS OVERLAYS

### Mass Wasting (overlay mw)

Areas where landforms suggest mass movement on unstable slopes, but where evidence for landslide deposits is inconclusive. Overlays encompass hummocky or irregular surface morphology, but boundaries of overlays generally lack unambiguous head scarps, lateral head scarps, or toes that unit Q<sub>1s</sub> may otherwise exhibit. We find that these mass wasting landforms are more common at higher elevations and may indicate areas of solifluction: gradual downslope mass movements related to freeze-thaw cycles.

### Quaternary Loess (overlay Q<sub>1</sub>)

Loess is light brown to medium brown; moderately weathered; low density, unconsolidated; composed of silt to very fine grained sand; angular; moderate sorting; internally structureless and forming 1-meter-tall, irregularly spaced mounds with varying amounts of post-depositional fluvial dissection. Loess is widespread in the map area and commonly blankets surfaces of older alluvial deposits—especially units Q<sub>af3</sub> and Q<sub>af4</sub>—and

bedrock. Loess is mostly absent on surfaces of younger alluvial deposits. Loess deposits are found on flat to gently sloping surfaces. The deposits are not tectonically folded, and generally, but not always, conceal faults that cut through bedrock. On the map we do not show faults mapped through loess as concealed. This is not meant to indicate that there is tectonic offset of the loess. Loess deposits in the map area are generally less than 3 m thick at a maximum and on average around 0.6–1.5 m thick. Local residents call loess mounds “Manastash Mounds” or more generally “patterned ground”, and they are interpreted to result from frost action under a periglacial climate (Kaatz, 1959; Williams and Masson, 1949). Anastomosing surface textures with ~0.3–1 m deep incisions that are ~0.6–5 m wide suggest that fluvial incision and erosion may also aid generation or modification of these mound landforms. This deposit correlates with the eolian loess of the Palouse Formation. Age is inferred to be approximately Holocene to Late Pleistocene based on correlation with the Palouse Formation.

### Miocene Hyaloclastite (overlay hy)

Hyaloclastite is a volcanoclastic aggregate consisting of pillow breccia with volcanic glass and its weathering product palagonite; light yellowish brown to orange brown or tan and generally strongly weathered; less dense than basalt, moderately well consolidated; generally composed of sand- to boulder-sized clasts in a very fine grained matrix; angular to subangular; poorly sorted; some exposures may contain cobble- to boulder-sized fragments of basalt pillows (cm- to m-scale) that are matrix supported (pillow breccia). Where pillows are absent, exposures are convoluted and structureless; pillow fragments have chilled margins and radial interior jointing akin to entablature. Vesicles are common in this basaltic material and where present are also called pillow, palagonite, vesicular complexes (PPVC). These volcanoclastic aggregates diagnostically include basaltic glass (tachylyte ± sideromelane), palagonite, and plagioclase crystals. Thickness varies but is generally less than 30 m where observed. Unit is most commonly found near the base of unit Mv<sub>gs</sub>mc and near the top of unit Mv<sub>go</sub>. Hyaloclastite is interpreted as resulting from the quenching of hot lava in water. The locations of hyaloclastites support the notion that these interactions occurred in lower paleotopographic elevations that preceded and followed the deposition of the Coleman member (unit Mc<sub>ec</sub>). These lithologic characteristics and spatial associations suggest that the hyaloclastite was locally generated from quenching with consequent fracturing, disintegration, and weathering of GRB lavas as they entered a Miocene water body. Exposures of hyaloclastite are small, isolated, and decrease eastward from Cooke Canyon, which we interpret as variations (discontinuities?) in the locations of waterbodies during the eruption of the Ortley (unit Mv<sub>go</sub>) and McCoy Canyon (unit Mv<sub>gs</sub>mc) compositional units. We did not observe peperitic hyaloclastite in the map area.

## SUMMARY OF GEOLOGIC STRUCTURES

Gently dipping stratigraphy typifies the central and northern parts of the map area, and dips steepen near the range front in the southern map area. We discuss structures near Whiskey ridge in the south as well as northerly striking faults.

## Geologic Structures Near Whiskey Ridge

The main structure along the range front in the map area is a more than 7.6-km long northwest-striking, northeast-side-up dextral(?)—reverse fault located southwest of Whiskey ridge. We informally name this structure the Whiskey ridge fault (WRF). We interpret this fault as connecting to a ~6.8 km-long, unnamed northwest-striking fault mapped to the west by Sadowski and others (2021) and we suspect the WRF splays into several strands in our southeastern map area and beyond. We estimate that the WRF has a total length of at least 14 km. We identify numerous, short fault segments and infer that they have small displacements near the Whiskey ridge fault. These short faults may be related to (1) mesoscale Riedel shears that support some amount of right-lateral slip on the WRF, (2) minor faulting and fracturing of basalt bedrock near the anticlinal hinge, (3) flow foliation parallel-slip (“bedding parallel-slip”), and (or) (4) a broader zone of brittle deformation not limited to the discrete WRF.

Folds associated with the WRF include Whiskey Dick anticline (WDA)—also called the ‘Cariboo anticline’ in Bentley (1977)—and Whiskey Jim syncline (WJS). Both the WDA and WJS were originally mapped and named—or renamed in WDA’s case—by Bentley and Powell in their unpublished field maps from the 1980s. Limbs of both named folds are open to gentle, and their fold axes are inferred to be cross cut by a north-northeast-striking fault in Park Creek. The orientations of these folds change across Park Creek, where west of Park Creek near Whiskey ridge they trend northwest and east of Park Creek away from Whiskey ridge they trend west. The Whiskey Ridge fault is flanked by a subparallel monocline–anticline–syncline group in its hangingwall, which we infer is related to slip on the Whiskey Ridge fault. Because of this relationship, we use the name Whiskey Dick anticline for the anticline along Whiskey ridge, though they may be separate folds.

We map two short monoclines on Whiskey ridge near these larger-scale folds, though their existence is only identified by sparse contact relationships among subunits of the Sentinel Bluffs Member. Additional geochemical data to classify the subunits of unit *Mvgs* may help refine fold geometries. Alternatively, faults may explain the relationships between these contacts, but we do not have additional geochemical data to identify repeated—or omitted—stratigraphy of the Sentinel Bluffs Member. We therefore cannot support a fault hypothesis despite the presence of several short fault segments nearby.

There is also a northwest-striking reverse fault between and subparallel to both the WRF and nearby syncline. It is identified from a pair of abruptly truncated basalt outcrops and changes in basalt geochemistry over short distances on the west side of Park Creek. We interpret this structure to be an antithetic fault and infer it has at least half of the offset found in the main structure. This south-side-up, antithetic fault is on trend with a shorter fault segment identified in a strath terrace of unit *Qaf4* to the northwest. We speculate that the sense of slip on this shorter fault is north-side-up based on local scarp morphology but we are not certain. Land access restrictions prevented us from assessing GRB geochemistry in the gap between these two faults and we are unable to determine if these faults connect or how they are related.

## Northerly Striking Faults (NSFs)

In the eastern half of the map area, we map numerous, short (<1.5-km-long) faults with north-northwest through north-northeast strikes. We infer that these faults have minimal meter-scale displacements and collectively refer to these structures as ‘northerly striking faults’ (NSFs), similar to Sadowski and others (2021). In other parts of the YFTB, such structures accommodate oblique slip (Bentley and Anderson, 1979; Bentley and Farooqui, 1979), so we infer that NSFs in the map area may also be oblique-slip faults.

In Park Creek, one of these structures is a ~4.8-km-long north-northeast-striking oblique(?)—slip fault that we measured as having less than ~30 m of down-to-the-west throw based on elevation differences of bedrock contacts on either side of the canyon (usually between 10–20 m for the bottom of unit *Mvgs*). Bedrock contact elevation differences decrease northward along the fault.

Many short NSFs in the central to eastern map area are in the western limb of a 60+ km long, regional, northerly trending fold: the Hog Ranch–Naneum anticline (HRNA) (Campbell, 1989; Reidel and others, 1989). In addition, the short NSFs have strikes that are subparallel to the trend of the HRNA fold axis, and the short NSFs and the HRNA both deform GRB rocks of the same ages. Given those observations, the short NSFs and this regional fold may be related. Possible explanations for a relationship between the NSFs and the anticline may include the following: (1) short, discontinuous NSFs in the map area may locally represent smaller-scale extensional fractures and faulting parallel to the crest of the HRNA; (2) short NSFs may be surface manifestations of a deep, northerly striking blind fault(s) whose slip may decrease up-dip; and (or) (3) alternatively, the short NSFs may represent younger, brittle deformation related to the regional on-going stress regime since the Miocene and NSFs have no relationship to deformation related to the HRNA.

Many short NSFs are also near the northerly-trending segments of the deep canyons containing Caribou and Park Creeks. Caribou Creek is in the deepest canyon (roughly 300+ m deep) in the map area and has a large bend of ~130° counterclockwise from north–northeast to west–southwest (025° through 255°). Park Creek is in the next deepest canyon (roughly 240 m deep), and it has a similarly shaped large bend (NNW through SW) located outside the map area to the east. These deep canyons are also west of the HRNA fold axis. Away from the anticlinal axis the canyons are orthogonal to its trend, but become more northerly closer to the axis. The orientation of the canyons relative to the HRNA fold axis may indicate that the fold and (or) the NSFs may impose some structural control on the orientation of the upper canyons.

## DISCUSSION OF GEOPHYSICS

Our geophysical anomaly map (Figure M1A) shows observed gravity and aeromagnetic anomalies within and near the map area. We also present our interpreted geophysical model (Figure M1B) that best fits the observed gravity and aeromagnetic geophysical data.

Gravity gradients that are large (>1.0 mGal) over short distances (<2 km) and straight over longer distances could



be associated with faults. The gradients we observe in the map area are overall quite low-amplitude compared to other gravity gradients elsewhere in Kittitas Valley and range from ~1.0–2.5 mGal in our map area. The largest amplitude gravity gradient (~2.5 mGal, WR gradient label in Figure M1A) in the map area is associated with mapped faults near Whiskey ridge and is more apparent on the model (near labels WRF and WDA on Figure M1B) than in map view. There are straight, moderate gravity gradients (~1.5–2.0 mGal) with contours subparallel to Park Creek (PC gradient label on Figure M1A) where we map a concealed fault, and subparallel to Cooke Creek (CC gradient label on Figure M1A) where we suspect a fault but lacked supporting geologic data within the map area. There is a moderate gravity gradient (~2.0 mGal) with gently curving gravity contours located along Whiskey Jim Creek (WJC gradient label on Figure M1A) where we map a west-trending pair of folds at the surface, but not a fault. However, at depth, a west-striking blind fault associated with the WJC gradient may be present, but our model doesn't cross this area so we are uncertain. If this blind fault exists, we speculate that it may be related to the Frenchman Hills thrust mapped farther east that trends toward Whiskey Jim Creek.

The prominent, linear aeromagnetic feature in the southwestern portion of the quadrangle is a northwest-trending relative magnetic low (blue colors on Figure M1A; likely caused by reversed magnetic remanence rocks at or near the surface) that coincides with the gravity gradient of the WRF (label WRF on Figure M1A). Geologic mapping and modeling agree on the location of the WRF and, like other faults in northern Kittitas Valley, it is associated with a linear magnetic lows (mentioned above). Given the geologic context of the area, this magnetic low is likely sourced by uplift of deep members of the GRB with reverse remanence in the cores of fault-related anticlines (WDA). We model this structure as a ~45° north-dipping fault with ~35 m of throw (~40–50 m of dip-slip displacement); our modeling does not constrain any strike-slip offset. Alternative models were generated to explore shallower fault dips and varying amounts of fault offset, however compared to observed geophysical anomalies, shallow dips caused calculated gravitational discrepancies south of the WDA in the vicinity of the footwall, while increasing offsets caused calculated magnetic discrepancies in the vicinity of the hanging wall. Northeast of the WRF, there is a broad, relative magnetic low (BML label on Figure M1) with inset smaller-amplitude, shorter wavelength magnetic and gravity gradients (upper two panels of Figure M1B under bracket of BML label). We model this broad magnetic low as a sequence of thicker packages with reverse magnetic remanence present in the subsurface. We interpret these thicker, reversely magnetized packages as having filled accommodation space that formed adjacent to very steeply north-dipping blind faults (normal or possibly oblique) during eruption of the GRB R2 MSU (Grouse Creek, Wapshilla Ridge, and Mt. Horrible members). We infer these blind faults to be transtensive structures that formed half-grabens in which GRB magnetostratigraphic units below N2 are thicker. The model we present also strongly suggests offset on pre-Miocene rocks to match observed anomalies.

Our modeling suggests GRB thickness variations at depth and in turn introduces thickness discrepancies with nearby subsurface data and with modeling by others (discussed in

more detail below). Firstly, our model suggests thinning of the Ortley member over the WDA, which we attribute to erosion and active deformation (uplift and folding) during the eruption of the Ortley member (unit **Mvgo**). Attempts to generate models that honor observed thicknesses of the Ortley member—similar to thicknesses we observe in the northeast where exposed—produce short wavelength mismatches between the calculated and observed magnetic data. In order to match observed magnetic anomalies in the vicinity of the WDA, uplift of the reversed Grouse Creek member (unit **Mvgg**) is needed, and because the Sentinel Bluff Member is observed at the surface, the Ortley member must be thinned. This implies that the WRF was active during the eruption of the Ortley member.

Secondly, the CRBG thickness we indicate on Figure M1B (~2,740 m thick) is more than that interpreted in the nearby BISSA 1-29 well (~1,400 m (4,600 ft) thick, located >8 km from the model) and is similar to or greater than nearby estimates from models by Blakely and others (2011) and Staisch and others (2018a). In the BISSA well, GRB R1 MSU is absent and a partial thickness of GRB N1 MSU is present (S. Reidel, WSU Tri-Cities, written commun., 2022). We attempted to resolve our model's thickness differences with the BISSA well but alternative geophysical models with absent R1 or thinner N1 basalt were unable to satisfy both potential-fields data while honoring surficial observations. Geologic explanations for our greater CRBG thickness estimates are not clear. Possible explanations for our greater CRBG thicknesses include: (1) the BISSA well is located near the crest of an anticline (HRNA) that, if active in the Miocene, could have affected thickness; (2) there are known faults between our model profile and the BISSA well, so our model may be in a different fault block; (3) our model uses measured thicknesses of GRB at the surface—especially for Sentinel Bluffs and Ortley members—that may impose greater thicknesses on older GRB units; and (or) (4) the presence of a package of unknown dense material with reversed magnetism (possibly the Teanaway basalt, see model of Sadowski and others, 2021) that is unaccounted for in our modeling. Regarding option four, without the Teanaway basalt, our model strongly suggests thicker GRB members. An alternative geophysical model that honors GRB thicknesses from the BISSA well could possibly match the observed geophysical data, however our attempts induce near-surface thicknesses that disagree with thickness results from surficial mapping.

Regarding alternative models to the moderately dipping WRF geometry we present, we also tried to generate a model exhibiting low-angle thrust fault geometries for the WRF but failed to match our observed aeromagnetic anomalies. In this failed model, varying the elevation of the pre-Eocene rocks could account for the absence of R1 and thinner N1 (to agree with BISSA well findings), but adjusting pre-Eocene contacts while removing R1 and adjusting N1 insufficiently accounted for the shorter wavelength aeromagnetic anomalies, which should be sourced from closer to the surface. In other words, our calculated aeromagnetic values are too great and do not fit our observed anomalies. To account for those higher-amplitude short-wavelength anomalies, modeling strongly suggests thicker packages of R2 and thinner packages of N2 than we observe in surface exposures. In conclusion, thicker packages of CRBG

with moderately dipping reverse fault geometry are strongly suggested to produce a model that best fits the observed potential field data while honoring surficial geologic observations.

## AGE OF FAULTING

Evidence for Quaternary faulting includes short, west- and northwest-trending fault scarps in unit Qaf3 east of the mouth of Park Creek and in unit Qaf4 on the strath terrace near Caribou Creek near the western map boundary. These scarps are likely related to deformation associated with the northwest-striking Whiskey ridge fault. Twenty-two kilometers to the west–northwest there are also fault scarps in unit Qaf3, which Sadowski and others (2020) date to ~470 ka. If the scarps in unit Qaf3 in our current map area are the same age, then the 35 m of offset we determine results in a slip rate of approximately 0.07 mm/yr, which is about 20 percent of the slip rate determined by Staisch and others (2018a) on the frontal fault just north of Manastash Ridge, about 17 km southwest of the map area. We recommend further investigation of fault scarps associated with the WRF to assess seismic hazard. Scarps related to northwest-striking faults and short NSFs may provide additional evidence for recent faulting, where those faults cross thin deposits of colluvium (unmapped) or loess (geologic overlay Ql) on Miocene basalt units. Such evidence is scarce and may be inadequate for assessing age of faulting.

## RECOMMENDATIONS FOR FUTURE RESEARCH

- Assess fault scarps in Quaternary and Tertiary deposits. Escarpments related to the Whiskey ridge fault east of Park Creek in the southern map area or west of Caribou Creek should be evaluated in more detail to assess their age, recent activity, and offset using ground penetrating radar (GPR), paleoseismic trenching, and more detailed surficial mapping of alluvial, colluvial, and eolian deposits. This would depend on permission from private landowners to access their land. Similarly, short NSFs could be evaluated for recent faulting where they disturb young colluvium or loess mounds.
- Paleomagnetic evaluation of possible fault block rotations near Whiskey ridge. Folds near Whiskey ridge may have been rotated in their respective fault blocks. A paleomagnetic investigation may elucidate this structural hypothesis.
- Compile geochemical and petrographic data of CRBG units. Organizing results across Kittitas County to refine geochemical compositional fields and microscopic characteristics will enhance existing understanding of local CRBG units and may aid in distinguishing aphyric units in the field.

## ACKNOWLEDGMENTS

We thank, from CWU: Nick Zentner, Walter Szeliga, Lisa Ely, Bre MacInnes, Angela Halfpenny, and many faculty of the Geology Department for many meaningful conversations and field trips.

From WGS, we thank: Maria Furtney and Emilie Richards for their help in the field. Also from WGS, we thank Alex Steely, Michael Polenz, Megan Anderson, and Katie Alexander for initial reviews of the map, cross section, and report text. From USGS, we thank Steve Angster and Lydia Staisch for help synthesizing past and on-going regional work. Of emeritus investigators, we thank Jack Powell, Steve Reidel, and Rick Conrey for clarifying structural and stratigraphic questions. Of WSU, thanks to Ashley Steiner, John Wolff, and the whole staff at the WSU Peter Hooper GeoAnalytical lab in Pullman, WA for analyzing geochemistry samples and classifying CRBG rocks using their Machine Learning (ML) model. Also from WSU, thanks to Jeff Vervoort and Vic Valencia (ZirChron LLC) for analyzing our detrital zircon samples in the Radiogenic Isotope and Geochronology Laboratory (RIGL).

Of private citizens, we thank John Lasher, Mr. and Mrs. Weber, Vijay Doshi, Andy Anderson, and a helpful retired CWU provost, all the folks associated with the Elkhorn Ranch Conservancy and the Secret Canyon gated community, and countless other private landowners, ranchers, cowboys and cowgirls, and businesses for general assistance or land access.

We also thank the PSE Wild Horse Wind & Solar Facility, the Kittitas Reclamation District (KRD), Poison Springs LLC, and Western WA Operating Engineers for access through or around their properties.

## AUTHOR CONTRIBUTIONS

Geologic mapping was performed by A. Sadowski with a week of assistance from M. Furtney and E. Richards. Gravity data were collected by T. Lau and geophysical data were interpreted and modeled by T. Lau. Writing of the pamphlet was completed by A. Sadowski with contributions from T. Lau in the *Methods*, *Appendix*, and *Discussion of Geophysics* sections. K. Alexander assisted in populating the Data Supplement. GeMS data schema adoption was facilitated by K. Alexander and A. Cabibbo. Map GIS linework, population of the GeMS schema, geologic analysis, and geologic cross section construction was performed by A. Sadowski.

## REFERENCES

- Allmendinger, R. W.; Cardozo, Nestor; Fisher, D. M., 2012, Structural geology algorithms: Vectors and tensors: Cambridge University Press, 289 p.
- Barnes, D. F.; Oliver, H. W.; Robbins, S. L., 1969, Standardization of gravimeter calibrations in the geological survey: *Eos, Transactions American Geophysical Union*, v. 50, no. 10, p. 626–627. [<https://doi.org/10.1029/EO050i010p00526>]
- Bentley, R. D., 1977, Stratigraphy of the Yakima basalts and structural evolution of the Yakima ridges in the western Columbia Plateau. In Brown, E. H.; Ellis, R. C., editors, *Geology excursions in the Pacific Northwest*: Geological Society of America, p. 339–390.
- Bentley, R. D.; Anderson, J. L., 1979, Right lateral strike slip faults in the western Columbia Plateau [abstract]: Rockwell Hanford Operations RHO-BWI-SA-28-A, 6 p.
- Bentley, R. D.; Farooqui, S. M., 1979, Left-lateral, strike-slip Riedel shears in the Yakima Ridges, Columbia Plateau, Washington and Oregon [abstract]: Rockwell Hanford Operations RHO-BWI-SA-40-A, 2 p.

- Black, L. P.; Kamo, S. L.; Allen, C. M.; Davis, D. W.; Aleinikoff, J. N.; Valley, J. W.; Mundil, Roland; Campbell, I. H.; Korsch, R. J.; Williams, I. S.; Foudoulis, Chris, 2004, Improved  $^{206}\text{Pb}/^{238}\text{U}$  microprobe geochronology by the monitoring of a trace-element-related matrix effect; SHRIMP, ID-TIMS, ELA-ICP-MS and oxygen isotope documentation for a series of zircon standards: *Chemical Geology*, v. 205, no. 1–2, p. 115–140. [https://doi.org/10.1016/j.chemgeo.2004.01.003]
- Blakely, R. J.; Sherrod, B. L.; Weaver, C. S., 2020a, High-resolution aeromagnetic survey of the Wenatchee area, Washington: U.S. Geological Survey data release. [https://doi.org/10.5066/P9EURKIG]
- Blakely, R. J.; Sherrod, B. L.; Weaver, C. S., 2020b, High-resolution aeromagnetic survey of the Cle Elum area, Washington: U.S. Geological Survey data release. [https://doi.org/10.5066/P9C9MADW]
- Blakely, R. J.; Sherrod, B. L.; Weaver, C. S.; Wells, R. E.; Rohay, A. C.; Barnett, E. A.; Knepprath, N. E., 2011, Connecting the Yakima fold and thrust belt to active faults in the Puget Lowland, Washington: *Journal of Geophysical Research Solid Earth*, v. 116, no. B7, 33 p. [https://doi.org/10.1029/2010JB008091]
- Brocher, T. M.; Wells, R. E.; Lamb, A. P.; Weaver, C. S., 2017, Evidence for distributed clockwise rotation of the crust in the northwestern United States from fault geometries and focal mechanisms: *Tectonics*, v. 36, no. 5, p. 787–818. [https://doi.org/10.1002/2016TC004223]
- Campbell, N. P., 1989, Structural and stratigraphic interpretation of rocks under the Yakima fold belt, Columbia Basin, based on recent surface mapping and well data. In Reidel, S. P.; Hooper, P. R., editors, *Volcanism and tectonism in the Columbia River flood-basalt province*: Geological Society of America Special Paper 239, p. 209–222. [https://doi.org/10.1130/SPE239-p209]
- Cardozo, Nestor; Allmendinger, R. W., 2013, Spherical projections with OSXStereonet: *Computers & Geosciences*, v. 51, p. 193–205. [https://doi.org/10.1016/j.cageo.2012.07.021]
- Chang, Zhaoshan; Vervoort, J. D.; McClelland, W. C.; Knaack, Charles, 2006, U-Pb dating of zircon by LA-ICP-MS: *Geochemistry, Geophysics, Geosystems*, v. 7, no. 5, 14 p. [https://doi.org/10.1029/2005GC001100]
- Czajkowski, J. L.; Bowman, J. D.; Schuster, J. E.; Wheeler, C. M., 2012, Oil and gas wells in Washington State: Washington Division of Geology and Earth Resources Open File Report 2012-02 (rev. 2015), 4 p., 1 Microsoft Excel file with 4 p. text. [http://www.dnr.wa.gov/Publications/ger\_ofr2012-02\_oil\_and\_gas\_wells.zip]
- Donaghy, E. E.; Umhoefer, P. J.; Eddy, M. P.; Miller, R. B.; LaCasse, Taylor, 2021, Stratigraphy, age, and provenance of the Eocene Chumstick basin, Washington Cascades; implications for paleogeography, regional tectonics, and development of strike-slip basins: *Geological Society of America Bulletin*, v. 133, no. 11–12, p. 2418–2438. [https://doi.org/10.1130/B35738.1]
- Ebinghaus, Alena; Jolley, D. W.; Hartley, A. J., 2015, Extrinsic forcing of plant ecosystems in a large igneous province: The Columbia River flood basalt province, Washington State, USA: *Geology*, v. 43, no. 12, p. 1107–1110. [https://doi.org/10.1130/G37276.1]
- Eddy, M. P.; Bowring, S. A.; Umhoefer, P. J.; Miller, R. B.; McLean, N. M.; Donaghy, E. E., 2016, High-resolution temporal and stratigraphic record of Siletzia's accretion and triple junction migration from nonmarine sedimentary basins in central and western Washington: *Geological Society of America Bulletin*, v. 128, no. 3–4, p. 425–441. [https://doi.org/10.1130/B31335.1]
- Eddy, M. P.; Umhoefer, P. J.; Miller, R. B.; Donaghy, E. E.; Gundersen, Melissa; Senes, F. I., 2017, Sedimentary, volcanic, and structural processes during triple-junction migration: Insights from the Paleogene record in central Washington. In Haugerud, R. A.; Kelsey, H. M., editors, *From the Puget Lowland to east of the Cascade Range: Geologic excursions in the Pacific Northwest*: Geological Society of America Field Guide 49, p. 143–174. [https://doi.org/10.1130/2017.0049(07)]
- Hammond, P. E., 2013, Distribution, stratigraphy, and structure of the Grande Ronde Basalt in the upper Naches River basin, Yakima and Kittitas Counties, Washington. In Reidel, S. P.; Camp, V. E.; Ross, M. E.; Wolff, J. A.; Martin, B. S.; Tolan, T. L.; Wells, R. E., editors, *The Columbia River flood basalt province: Geological Society of America Special Paper 497*, p. 363–400. [https://doi.org/10.1130/2013.2497(15)]
- Heiskanen, W. A.; Vening-Meinesz, F. A., 1958, *The Earth and its gravity field*: McGraw-Hill Book Company, Inc., 470 p.
- Hoyt, C. L., 1961, The Hammond sill—An intrusion in the Yakima Basalt near Wenatchee, Washington: *Northwest Science*, v. 35, no. 2, p. 58–64.
- International Union of Geodesy and Geophysics, 1971, Geodetic reference system 1967: International Association of Geodesy Special Publication no. 3, 116 p.
- Jachens, R. C.; Roberts, C. R., 1981, Documentation of a FORTRAN program, 'isocomp', for computing isostatic residual gravity: U.S. Geological Survey Open-File Report 81-574, 26 p. [https://doi.org/10.3133/ofr81574]
- Johnson, S. Y., 1985, Eocene strike-slip faulting and nonmarine basin formation in Washington. In Biddle, K. T.; Christie-Blick, Nicholas, editors, *Strike-slip deformation, basin formation, and sedimentation*: Society of Economic Paleontologists and Mineralogists Society for Sedimentary Geology Special Publication 37, p. 283–302. [https://doi.org/10.2110/pec.85.37.0265]
- Kaatz, M. R., 1959, Patterned ground in central Washington; A preliminary report: *Northwest Science*, v. 33, no. 4, p. 145–156.
- Kasbohm, Jennifer; Schoene, Blair, 2018, Rapid eruption of the Columbia River flood basalt and correlation with the mid-Miocene climate optimum: *Science Advances*, v. 4, no. 9, 8 p. [https://doi.org/10.1126/sciadv.aat8223]
- Kelsey, H. M.; Ladinsky, T. C.; Staisch, Lydia; Sherrod, B. L.; Blakely, R. J.; Pratt, T. L.; Stephenson, W. J.; Odum, J. K.; Wan, Elmira, 2017, The story of a Yakima fold and how it informs late Neogene and Quaternary backarc deformation in the Cascadia subduction zone, Manastash anticline, Washington, USA: *Tectonics*, v. 36, no. 10, p. 2085–2107. [https://doi.org/10.1002/2017TC004558]
- PSLC, 2011, Kittitas study area 2011 project, collected between Sept. 15 and Nov. 5, 2010 by Watershed Sciences, Inc., 3-ft resolution, accessed Aug. 31, 2020 [http://lidarportal.dnr.wa.gov/], data available on portal [ger\_kittitas\_2011\_lidar\_report.pdf].
- Lanphere, M. A.; Baadsgaard, Halfdan, 2001, Precise K–Ar,  $^{40}\text{Ar}/^{39}\text{Ar}$ , Rb–Sr and U/Pb mineral ages from the 27.5 Ma Fish Canyon Tuff reference standard: *Chemical Geology*, v. 175, no. 3–4, p. 653–671. [https://doi.org/10.1016/S0009-2541(00)00291-6]
- Ludwig, K. R., 2012, Isoplot 3.75: A geochronological toolkit for Microsoft Excel: Berkeley Geochronological Center Special Publication no. 5, 75 p.
- McCaffrey, Robert; King, R. W.; Payne, S. J.; Lancaster, Matthew, 2013, Active tectonics of northwestern U. S. inferred from GPS-derived surface velocities: *Journal of Geophysical Research Solid Earth*, v. 118, no. 2, p. 709–723. [https://doi.org/10.1029/2012JB009473]
- McDonald, E. V.; Busacca, A. J., 1992, Late Quaternary stratigraphy of loess in the Channeled Scabland and Palouse regions of Washington State: *Quaternary Research*, v. 38, no. 2, p. 141–156. [https://doi.org/10.1016/0033-5894(92)90052-K]
- McMillan, Kent; Long, P. E.; Cross, R. W., 1989, Vesiculation in Columbia River Basalts. In Reidel, S. P.; Hooper, P. R., editors, *Volcanism and tectonism in the Columbia River flood-basalt province*: Geological Society of America Special Paper 239, p. 157–167. [https://doi.org/10.1130/SPE239-p157]



- Morelli, Carlo; Gantar, C.; Honkasalo, Tauno; McConnel, R. K.; Tanner, J. G.; Szabo, Bela; Uotila, Urho; Whalen, C. T., 1974, The international gravity standardization net 1971 (IGSN71): International Association of Geodesy Special Publication No. 4, 194 p.
- Nilsen, T. H., 1976, Washington gravity base station network: Washington Division of Geology and Earth Resources Information Circular 59, 83 p.
- Paces, J. B.; Miller J. D., Jr., 1993, Precise U-Pb ages of Duluth Complex and related mafic intrusions, northeastern Minnesota: Geochronological insights to physical, petrogenetic, paleomagnetic, and tectonomagmatic processes associated with the 1.1 Ga Midcontinent Rift System: *Journal of Geophysical Research*, v. 98, no. B8, p. 13,997–14,013. [https://doi.org/10.1029/93JB01159]
- Paton, Chad; Hellstrom, John; Paul, Bence; Woodhead, Jon; Hergt, Janet, 2011, Iolite: Freeware for the visualization and processing of mass spectrometric data: *Journal of Analytical Atomic Spectrometry*, v. 26, p. 2508–2518. [https://doi.org/10.1039/C1JA10172B]
- Plouff, D., 2000, Field estimates of gravity terrain corrections and Y2K-compatible method to convert from gravity readings with multiple base stations to tide- and long-term drift-corrected observations: U.S. Geological Survey Open-File Report 00-140, 37 p. [https://pubs.usgs.gov/of/2000/0140/]
- Porter, S. C., 1976, Pleistocene glaciation in the southern part of the north Cascade Range, Washington: *Geological Society of America Bulletin*, v. 87, no. 1, p. 61–75. [https://doi.org/10.1130/0016-7606(1976)87<61:PGITSP>2.0.CO;2]
- Reidel, S. P., 2005, A lava flow without a source: The Cohasset flow and its compositional components, Sentinel Bluffs Member, Columbia River Basalt Group: *Journal of Geology*, v. 113, no. 1, p. 1–21. [https://doi.org/10.1086/425966]
- Reidel, S. P., 2015, Igneous rock associations 15. The Columbia River Basalt Group: A flood basalt province in the Pacific Northwest, USA: *Geoscience Canada*, v. 42, no. 1, p. 151–168.
- Reidel, S. P.; Scott, G. R.; Bazard, D. R.; Cross, R. W.; Dick, Brian, 1984, Post-12 million year clockwise rotation in the central Columbia Plateau, Washington: *Tectonics*, v. 3, no. 2, p. 251–273. [https://doi.org/10.1029/TC003i002p00251]
- Reidel, S. P.; Tolan, T. L., 2013, The Grande Ronde Basalt, Columbia River Basalt Group. In Reidel, S. P.; Camp, V. E.; Ross, M. E.; Wolff, J. A.; Martin, B. S.; Tolan, T. L.; Wells, R. E., editors, *The Columbia River flood basalt province: Geological Society of America Special Paper 497*, p. 117–154. [https://doi.org/10.1130/2013.2497(05)]
- Reidel, S. P.; Fecht, K. R.; Hagood, M. C.; Tolan, T. L., 1989, The geologic evolution of the central Columbia Plateau. In Reidel, S. P.; Hooper, P. R., editors, *Volcanism and tectonism in the Columbia River flood-basalt province: Geological Society of America Special Paper 239*, p. 247–264. [https://doi.org/10.1130/SPE239-p247]
- Reidel, S. P.; Camp, V. E.; Tolan, T. L.; Martin, B. S., 2013a, The Columbia River flood basalt province: Stratigraphy, areal extent, volume, and physical volcanology. In Reidel, S. P.; Camp, V. E.; Ross, M. E.; Wolff, J. A.; Martin, B. S.; Tolan, T. L.; Wells, R. E., editors, *The Columbia River flood basalt province: Geological Society of America Special Paper 497*, p. 1–44. [https://doi.org/10.1130/2013.2497(01)]
- Reidel, S. P.; Camp, V. E.; Tolan, T. L.; Kauffman, J. D.; Garwood, D. L., 2013b, Tectonic evolution of the Columbia River flood basalt province. In Reidel, S. P.; Camp, V. E.; Ross, M. E.; Wolff, J. A.; Martin, B. S.; Tolan, T. L.; Wells, R. E., editors, *The Columbia River flood basalt province: Geological Society of America Special Paper 497*, p. 293–324. [https://doi.org/10.1130/2013.2497(12)]
- Rosenmeier, F. J., 1968, Stratigraphy and structure of the Table Mountain–Mission Peak area in the Wenatchee Mountains, central Washington: University of Washington Master of Science thesis, 44 p., 1 plate.
- Sadowski, A. J.; Gilliland, A. L.; Anderson, M. L., 2021, Geologic map of the Colockum Pass SW and southern half of the Naneum Canyon 7.5-minute quadrangles, Kittitas County, Washington: Washington Geological Survey Map Series 2021-03, 1 sheet, scale 1:24,000, 23 p. text. [https://www.dnr.wa.gov/publications/ger\_ms2021-03\_geol\_map\_colockum\_pass\_sw\_southern\_naneum\_canyon\_24k.zip]
- Sadowski, A. J.; McCosby, J. B.; Anderson, M. L.; Lau, T. R.; Steiner, Ashley; DuFrane, S. A.; Rittenour, Tammy; Housen, Bernard, 2020, Geologic map of the Ellensburg North and southern half of the Reecer Canyon 7.5-minute quadrangles, Kittitas County, Washington: Washington Geological Survey Map Series 2020-01, 1 sheet, scale 1:24,000, 25 p. text. [https://www.dnr.wa.gov/publications/ger\_ms2020-01\_geol\_map\_ellensburg\_north\_reecer\_canyon\_24k.zip]
- Sawlan, M. G., 2018, Alteration, mass analysis, and magmatic composition of the Sentinel Bluffs Member, Columbia River flood basalt province: *Geosphere*, v. 14, no. 1, 18 p. [https://doi.org/10.1130/GES01188.1]
- Schmincke, Hans-Ulrich, 1964, Petrology, paleocurrents, and stratigraphy of the Ellensburg Formation and interbedded Yakima Basalt flows, south-central Washington: Johns Hopkins University Doctor of Philosophy thesis, 426 p.
- Schmincke, Hans-Ulrich, 1967, Stratigraphy and petrography of four upper Yakima Basalt flows in south-central Washington: *Geological Society of America Bulletin*, v. 78, no. 11, p. 1385–1422. [https://doi.org/10.1130/0016-7606(1967)78[1385:SAPOFU]2.0.CO;2]
- Schuster, J. E., compiler, 1994, Geologic map of the east half of the Yakima 1:100,000 quadrangle, Washington: Washington Division of Geology and Earth Resources Open File Report 94-12, 19 p., 1 plate. [https://www.dnr.wa.gov/Publications/ger\_ofr94-12\_geol\_map\_yakima\_e\_100k.zip]
- Sláma, Jiří; Košler, Jan; Condon, D. J.; Crowley, J. L.; Gerdes, Alex; Hanchar, J. M.; Horstwood, M. S. A.; Morris, G. A.; Nasdala, Lutz; Norberg, Nicholas; Schaltegger, Urs; Schoene, Blair; Tubrett, M. N.; Whitehouse, M. J., 2008, Plešovice zircon—A new natural reference material for U-Pb and Hf isotopic microanalysis: *Chemical Geology*, v. 249, no. 1-2, p. 1–35. [https://doi.org/10.1016/j.chemgeo.2007.11.005]
- Smith, G. A., 1988a, Neogene synvolcanic and syntectonic sedimentation in central Washington: *Geological Society of America Bulletin*, v. 100, no. 9, p. 1479–1492. [https://doi.org/10.1130/0016-7606(1988)100<1479:NSASSI>2.3.CO;2]
- Smith, G. A., 1988b, Sedimentology of proximal to distal volcanics dispersed across an active foldbelt: Ellensburg Formation (late Miocene), central Washington: *Sedimentology*, v. 35, no. 6, p. 953–977. [https://doi.org/10.1111/j.1365-3091.1988.tb01740.x]
- Smith, G. O., 1903a, Geologic atlas of the United States—Ellensburg folio, Washington: U.S. Geological Survey Geologic Folio 86, 7 p., with maps, scale 1:125,000.
- Smith, G. O., 1903b, Anticlinal mountain ridges in central Washington: *Journal of Geology*, v. 11, no. 2, p. 166–177. [https://www.journals.uchicago.edu/doi/pdf/10.1086/621067]
- Staisch, Lydia; Blakely, Richard; Kelsey, Harvey; Styron, Richard; Sherrod, Brian, 2018a, Crustal structure and Quaternary acceleration of deformation rates in central Washington revealed by stream profile inversion, potential field geophysics, and structural geology of the Yakima folds: *Tectonics*, v. 37, no. 6, p. 1750–1770. [https://doi.org/10.1029/2017TC004916]
- Staisch, Lydia; Kelsey, Harvey; Sherrod, Brian; Moller, Andreas; Paces, James; Blakely, Richard; Styron, Richard, 2018b, Miocene–Pleistocene deformation of the Saddle Mountains: Implications for seismic hazard in central Washington, USA: *Geological Society of America Bulletin*, v. 130, no. 3–4, p. 411–437. [https://doi.org/10.1130/B31783.1]

- Swanson, D. A.; Wright, T. L., 1976, Guide to field trip between Pasco and Pullman, Washington, emphasizing stratigraphy, vent areas, and intracanyon flows of Yakima Basalt; Geological Society of America Cordilleran Section, 72nd Annual Meeting, Field guide no. 1: Washington State University Department of Geology, 33 p.
- Swanson, D. A.; Wright, T. L., 1978, Bedrock geology of the northern Columbia Plateau and adjacent areas. *In* Baker, V. R.; Nummedal, Dag, editors, The channeled scablands—A guide to the geomorphology of the Columbia Basin, Washington: U.S. National Aeronautics and Space Administration, p. 37-57.
- Swick, C. H., 1942, Pendulum gravity measurements and isostatic reductions: U.S. Department of Commerce Coast and Geodetic Survey Special Publication 232, 82 p.
- Tabor, R. W.; Waitt, R. B., Jr.; Frizzell, V. A., Jr.; Swanson, D. A.; Byerly, G. R.; Bentley, R. D., 1982, Geologic map of the Wenatchee 1:100,000 quadrangle, central Washington: U.S. Geological Survey Miscellaneous Investigations Series Map I-1311, 1 sheet, scale 1:100,000, with 26 p. text. [<https://doi.org/10.3133/i1311>]
- Telford, W. M.; Geldart, L. O.; Sheriff, R. E., 1990, Applied Geophysics: New York, Cambridge University Press, 770 p.
- WA DNR, 2014, Colockum 2014 project, collected between Jun. 25 and Jul. 6, 2014 by Geoterra 3Di Mapping, Inc., 3-ft resolution, accessed Aug. 31, 2020 [<http://lidarportal.dnr.wa.gov/>], metadata available on portal [[ger\\_colockum\\_2014\\_lidar\\_report.pdf](#)].
- Waitt, R. B., Jr., 1979, Late Cenozoic deposits, landforms, stratigraphy, and tectonism in Kittitas Valley, Washington: U.S. Geological Survey Professional Paper 1127, 18 p. [<https://doi.org/10.3133/pp1127>]
- Wells, R. E.; McCaffrey, Robert, 2013, Steady rotation of the Cascade arc: *Geology*, v. 41, no. 9, p. 1027–1030. [<https://doi.org/10.1130/G34514.1>]
- Wells, R. E.; Weaver, C. S.; Blakely, R. J., 1998, Fore-arc migration in Cascadia and its neotectonic significance: *Geology*, v. 26, no. 8, p. 759–762. [[https://doi.org/10.1130/0091-7613\(1998\)026<0759:FAMICA>2.3.CO;2](https://doi.org/10.1130/0091-7613(1998)026<0759:FAMICA>2.3.CO;2)]
- Wiedenbeck, Michael; Allé, P.; Corfu, Fernando; Griffin, W. L.; Meier, Martin; Oberli, Felix; Von Quadt, Albrecht; Roddick, J. C.; Spiegel, W., 1995, Three natural zircon standards for U-Th-Pb, Lu-Hf, trace element and REE analyses: *Geostandards Newsletters*, v. 19, p. 1–23. [<https://doi.org/10.1111/j.1751-908X.1995.tb00147.x>]
- Williams, I. S., 1998, U-Th-Pb geochronology by ion microprobe: *In* M.A. McKibben, W.C. Shanks III, W.I. Ridley, editors, Applications of microanalytical techniques to understanding mineralizing processes: *Reviews in Economic Geology*, v. 7, p. 1–35. [<https://doi.org/10.5382/Rev.07>]
- Williams, Howel; Masson, P. H., 1949, Geology of the Macdoel quadrangle and circular soil structures in northeastern California: California Division of Mines and Geology, Bulletin 151, scale 1:125,000. [[https://ngmdb.usgs.gov/Prodesc/proddesc\\_531.htm](https://ngmdb.usgs.gov/Prodesc/proddesc_531.htm)]
- Wilson, M. S.; Dyman, T. S.; Condon, S. M., 2008, Evaluation of welltest results and the potential for basin-center gas in the Columbia basin, central Washington: U.S. Geological Survey Data Series 2184-F-O, 12 p. [<https://doi.org/10.3133/ds2184FO>]

## Appendix A. Geophysics

### OVERVIEW

Lateral changes in isostatic gravity across a region result from density changes within rocks of the mid-to-upper crust. Gravity surveys are especially useful in delineating steeply dipping contacts between two rock bodies that have a large contrast in density. Areas of high gravity indicate that high-density rocks (for example, many igneous and metamorphic rocks) are closer to the surface. Areas of low gravity indicate less-dense material that results from near-surface, low-density sediments, such as in sedimentary basins. Gridding gravity measurements creates a map that outlines areas of high gravity and low gravity. Gravity data constrained with measured rock densities allow us to create models of the subsurface that quantitatively predict observed data.

### SAMPLE COLLECTION AND PREPARATION

Measurements from 849 gravity stations were collected from 2019–2021 using a Scintrex CG-6 meter (Serial # 19050174) and PACES (now defunct; data obtained from B. Drenth, U. S. Geological Survey, written communication, 2020). We utilized the Ellensburg B base station (Nilsen, 1976) to tie our data to the U.S. gravity network.

Gravity station spacing at roughly 2 km generates a basic grid over a large area. In areas where known structures exist or initial gravity data collection showed a significant gradient, station spacing is 1 km to provide greater resolution. Where available, 90 new bedrock density samples and magnetic susceptibility measurements collected from exposed bedrock provide ground-truth for map interpretation and constrain geophysical modeling at these locations.

### DATA CORRECTIONS AND PROCESSING

A Javad Triumph-2 differential GPS unit provided the horizontal and vertical position of each station. Horizontal positions are then used to pull elevations from lidar where available. We apply the factory instrument (gravimeter) calibration constants to each gravity observation, apply correction factors obtained from the Mount Hamilton calibration loop east of San Jose, CA (Barnes and others, 1969), and correct for Earth tides to produce observed gravity values. The data reference the International Gravity Standardization Net of 1971 (Morelli, 1974), and the reference ellipsoid is the Geodetic Reference System of 1967 (International Association of Geodesy and Geophysics, 1971).

Gravity data reduction formulas for the free-air anomaly are standard (for example, Telford and others, 1990; Swick, 1942) and we applied Bouguer, Earth curvature, and terrain corrections out to 166.7 km from each station to produce a complete Bouguer anomaly. Terrain corrections are a combination of a field-based component (to a radius of 68 m using the Hayford system; Plouff, 2000) and a computer-generated component (using National Elevation Dataset elevations; Don Plouff, U. S. Geological Survey, oral and written communication, 2019). The complete Bouguer anomaly is further reduced to an isostatic anomaly using an Airy-Heiskanen model (Heiskanen and Vening-Meinesz, 1958) that produces the isostatic correction, assuming a 25-km-thick crust at sea level and a crust-mantle density contrast of 400 kg/m<sup>3</sup>. All parts of the data reduction process assume a standard reduction density of 2,670 kg/m<sup>3</sup>. Average uncertainty in steep and hilly regions is 0.12–0.23 mGal, whereas average uncertainty in flatter areas is 0.05–0.1 mGal.

### RESULTS

The minimum curvature algorithms in the GIS software package Geosoft Oasis Montaj transform our point isostatic anomaly data into gridded surfaces, which we use to produce 0.5 mGal contours (Fig. M1A). Gravity data are available in the Data Supplement. We present one possible geophysical model in Figure M1B.

---

## Appendix B. Geochemistry

### OVERVIEW

We analyzed volcanic rocks in the map area according to their major and trace elements using whole-rock geochemistry as determined by X-Ray Fluorescence (XRF) only. This method allows us to determine rock elemental compositions and chemostratigraphic classifications. The results of the analyses are presented in the Data Supplement.

### SAMPLE COLLECTION AND PREPARATION

We collected 169 samples from the map area, representing a variety of CRBG volcanic cooling textures that includes: colonnades, entablatures, vesicular tops, hyaloclastites, platy entablature, and autobreccias. We focused on collecting the first three types, but we collected from the others where we had no better outcrop options.

The freshest available samples were collected from outcrops with a sledgehammer. All samples were field cleaned (knapped by hand or using local bedrock exposures as anvils). Weathering rinds were removed as much as possible in the field (>90% of samples). Additional weathering rind cleaning or sample splitting (<10%) was performed at the CWU rock preparation lab using a sledgehammer and steel plate (anvil). Removing weathering rinds—if present—from vesicular tops was not always possible. Samples contain varied amounts of weathering and (or) hydration seams and (or) alteration. Samples with secondary minerals were rarely collected. Weathered, hydrated, or altered samples were collected and analyzed where no fresher samples were available. In general, samples submitted to the lab ranged in size from centimeter-sized chips to fist-sized fragments.

Hydration seams (“alteration seams”, as described in Supplemental File 3 of Sawlan, 2018) were not rigorously removed before sending to WSU for further preparation: crushing, pulverization/powering, and glass-bead fusion. Laboratory-based sub-sampling (Sawlan, 2018) was not performed due to time-constraints. However, most samples are of inter-rind to inter-seam sample quality (Table S1 of Sawlan, 2018).

### DATA CORRECTIONS AND PROCESSING

We used the machine learning (ML) model developed by Dr. Ashley Steiner at the WSU Peter Hooper GeoAnalytical Lab to categorize GRB members, submembers, and formations without stratigraphic context. Overall, the model does a better job distinguishing formation-level units from each other (for example, Wanapum versus Grande Ronde) than member-level or submember-level units from each other. For this reason, we relied less on the ML model for member-level and submember-level classifications compared to previous years. Instead, we plotted elemental variation diagrams ( $\text{TiO}_2$  vs  $\text{MgO}$ ,  $\text{TiO}_2$  vs  $\text{P}_2\text{O}_5$ , and amounts of Zr and Cr) and used stratigraphic understanding to determine the most reasonable member and submember classifications, especially when ML classifications had low confidence values.

### RESULTS

Results for 169 samples are in this report’s Data Supplement. Limits of Determination (LOD) for each analyte are also included in the Data Supplement column header for each respective analyte.

## Appendix C. Geochronology

### OVERVIEW

We analyzed sedimentary material in the map area to determine maximum depositional age (MDA) and to conduct a preliminary assessment of the provenance of detrital zircons. For this year's study we collected samples at one location, Age Site GD01. Summary data for this site are contained in Table C1; individual zircon analytical results are in the Data Supplement.

### SAMPLE COLLECTION AND PREPARATION

To understand the ages of particular rock units, we collected samples for zircon age analysis. In general, we attempted to retrieve about 2–4 kg of fresh rock for each sample, making sure to minimize any contact with soil or other surface deposits, which could introduce anomalous zircons. The packaged samples were sent to ZirChron, LLC for mineral separation using the following procedure. Samples were pressure washed with water and then disaggregated using an Electro Pulse Disaggregator (EPD, Marx generator) at 1 Hz with discharges of ~250 kV for 15 minutes. Any clasts >500  $\mu\text{m}$  were crushed in a crusher or pulverizer. Using stainless steel sieves, the fraction between 350  $\mu\text{m}$  and 25  $\mu\text{m}$  was retained and then processed using the Wilfley water table, Frantz paramagnetic separator, and a two-step (3.00 g/cm<sup>3</sup> and 3.32 g/cm<sup>3</sup>) heavy liquid methylene iodide separation. Approximately 100 individual zircon grains from each sample were hand selected and mounted in epoxy, polished to expose the grain centers, and regions suitable for analysis were identified from optical imaging.

### ANALYTICAL METHODS

Zircon U-Pb ages from the map area were measured at the Radiogenic Isotope and Geochronology Lab (RIGL) at Washington State University using an Analyte G2 193 excimer laser ablation system coupled with a Thermo-Finnigan Element 2 single-collector inductively coupled plasma mass spectrometer. The laser parameters were 25  $\mu\text{m}$  in diameter spot size, 10 Hz repetition rate, and ~5.0 J/cm<sup>2</sup> fluence. For the U-Pb measurement, we mostly followed the method of Chang and others (2006), except for the use of the 193 nm laser system instead of the 213 nm laser. A 10-second blank measurement of the He and Ar carrier gases (laser off) before each analysis was followed by 250 scans across masses <sup>202</sup>Hg, <sup>204</sup>Pb+Hg, <sup>206</sup>Pb, <sup>207</sup>Pb, <sup>208</sup>Pb, <sup>232</sup>Th, <sup>235</sup>U, and <sup>238</sup>U during ~30-sec-long laser ablation periods (in other words, one continuous, 30-second ablation at 10 Hz—10 shots fired per second—for ~300 laser shots). Analyses of zircon unknowns, standards, and quality control zircon grains were interspersed with analyses of external calibration standards, typically with 10–12 unknowns bracketed by multiple analyses of two different zircon standards (Plešovice and FC-1). The Plešovice standard (337 Ma; Sláma and others, 2018) was used to calibrate the <sup>206</sup>Pb/<sup>238</sup>U and <sup>207</sup>Pb/<sup>235</sup>U ages, and the FC-1 standard (1,099 Ma; Paces and Miller, 1993) was used for calibration of <sup>207</sup>Pb/<sup>206</sup>Pb ages owing to its high count rate for <sup>207</sup>Pb (~2–4 times higher than that of Plešovice). Zircon 91500 (1,065 Ma; Wiedenbeck and others, 1995; n=28 <sup>207</sup>Pb/<sup>206</sup>Pb age=1,063 +2.4/-5.0 Ma), Fish Canyon Tuff (~27.5 Ma; Lanphere and Baadsgaard, 2001; n=35 <sup>206</sup>Pb/<sup>238</sup>U age=27.9 +.01/-0.2 Ma) and Temora2 (417 Ma; Black and others, 2004, n=48 <sup>206</sup>Pb/<sup>238</sup>U age=417.0 +1/-1 Ma) were used as quality control standards. Data were processed offline using the Iolite software (Paton and others, 2011). Common Pb correction was performed using the <sup>207</sup>Pb method (Williams, 1998). Plots were calculated using Isoplot 4.16 (Ludwig, 2012). Zircon U-Pb data are reported in the Data Supplement.

### RESULTS

The total samples collected and analyzed in 2021 (n=6) have results divided into two map areas: One result (site GD01) is from the Colockum Pass SE quadrangle (and nearby) and five results are from the East Kittitas quadrangle (and nearby). Analyses from the one sample site in the map area are reported here, whereas the remaining 5 results will be published as part of next year's mapping. Summary data for geochronology site GD01 results are contained in Table C1; individual zircon analytical results are in the Data Supplement.

**Table C1.** Detrital zircon maximum constraining ages from age sites GD3 and GD4. See Data Supplement for full analytical results.

<b>Site ID</b>	GD01	Specimen details: detrital sample from a dusty, dirtroad exposure (probably outcrop) about 30 ft above the active stream channel. Exposure appears to be outcrop of alluvial material onlapped onto Miocene outcrops. Possibly reworked or contaminated with younger grains given exposure setting. We analyzed light to medium gray sand that is unconsolidated, moderately > poorly sorted, mica-less, fine- to medium-grained (<0.5mm) angular plagioclase with lesser subrounded quartz. Material also contains common basalt lithic fragments (unanalyzed). Age considerations: abundance of zircon grains with ages less than 1 Ma strongly suggests a Quaternary age (<1 Ma?). 20 grain analyses were discarded by Dr. Valencia due to very low isotope values ("no secular equilibrium"). The youngest peak of the remaining 85 grains included 68 grains.
<b>Field sample ID</b>	Cpa025	
<b>Map unit</b>	Qia?	
<b>TRS location</b>	Sec. 14, T18N R20E	
<b>Latitude (degrees)</b>	47.047531	
<b>Longitude (degrees)</b>	-120.285744	
<b>Elevation (ft)</b>	330	
Age (Ma) $\pm 2\sigma$		0.28 $\pm$ 0.04 (weighted mean of youngest peak (n=68))



